UNIVERSITY OF SÃO PAULO
SÃO CARLOS SCHOOL OF ENGINEERING

LEONARDO HENRIQUE MARTINS FLORENTINO

A theoretical study of noise attenuation in a turbofan engine using Herschel-Quincke waveguides

São Carlos
2023

LEONARDO HENRIQUE MARTINS FLORENTINO

A theoretical study of noise attenuation in a turbofan engine using Herschel-Quincke waveguides

Monograph presented to the Aeronautical Engineering Course of São Carlos School of Engineering of University of São Paulo in partial fulfilment of the requirements for the degree of Aeronautical Engineer.

Advisor: Prof. Dr. Paulo Celso Greco Júnior

CORRECTED VERSION

São Carlos

2023

Catalog card prepared by Patron Service at “Prof. Dr. Sergio Rodrigues Fontes Library” at EESC/USP

Florentino, Leonardo Henrique Martins
F633t A theoretical study of noise attenuation in a turbofan engine using Herschel-Quincke waveguides / Leonardo Henrique Martins Florentino; advisor Paulo Celso Greco Júnior. -- São Carlos, 2023.

Monograph (Bachelor Thesis) – Undergraduate in Aeronautics Engineering. -- São Carlos School of Engineering, at University of São Paulo, 2023.

1. Aeroacoustics. 2. Mathematical physics. 3. Herschel-Quincke waveguides. 4. Noise attenuation. I. Título.

Prepared by Eduardo Graziosi Silva- CRB-8/8907

FOLHA DE APROVAÇÃO
Approval sheet

Candidato / *Student*: Leonardo Henrique Martins Florentino
Título do TCC / *Title* : A theoretical study of noise attenuation in a turbofan engine using Herschel-Quincke waveguides
Data de defesa / *Date*: 12/07/2023

Comissão Julgadora / *Examining committee*	**Resultado** / *result*
Professor Associado Marcello Augusto Faraco de Medeiros	Aprovado
Instituição / Affiliation: EESC - SAA	
Professor Titular Luiz Nunes de Oliveira	Aprovado
Instituição / Affiliation: IFSC - USP	

Presidente da Banca / Chair of the Examining Committee:

Professor Associado Marcello Augusto Faraco de Medeiros
(assinatura / *signature*)

ABSTRACT

MARTINS FLORENTINO, LEONARDO HENRIQUE. **A theoretical study of noise attenuation in a turbofan engine using Herschel-Quincke waveguides**. 2023. Monograph (Bachelor Final Thesis) - São Carlos School of Engineering, University of São Paulo, São Carlos, 2023.

This work aims to explain noise attenuation in a turbofan engine from physical theory through the use of a device called Herschel-Quincke (HQ) waveguide. It is demonstrated by Burdisso and Smith from experimental analysis that the use of the HQ waveguides at the inlet of the engine is capable to reduce significantly the noise generated by the turbofan engine. From this starting point, and utilising analogies from the electromagnetic theory of physics, the engine is modelled as a cylindrical waveguide. The equation for sound propagation on the cylindrical waveguide in this model is derived through Navier-Stokes equations. Afterwards, the differential equation for the pressure field in the waveguide is solved by separation of variables, what invites us the study of Bessel functions and its properties. Finally, in order to reproduce the effect of the HQ waveguide, an analogy with sound sources is employed, which shows, through acoustic and differential equation theory, the effect of energy confinement caused by the HQ waveguides and their role in reducing acoustic noise from leaving the turbofan engine. A conclusion is drawn from the study and improvements for future works are suggested.

Keywords: Aeroacoustics. Mathematical physics. Herschel-Quincke waveguides. Noise attenuation.

RESUMO

MARTINS FLORENTINO, LEONARDO HENRIQUE. **A theoretical study of noise attenuation in a turbofan engine using Herschel-Quincke waveguides**. 2023. Monografia (Trabalho de Conclusão de Curso) - Escola de Engenharia de São Carlos, Universidade de São Paulo, São Carlos, 2023.

Este trabalho busca explicar a atenuação de ruído em um motor turbofan a partir de conceitos físicos por meio do uso de um dispositivo chamado de guia de onda de Herschel-Quincke (HQ). Estudos experimentais feitos por Burdisso e Smith demonstram que o uso das guias de onda HQ na entrada do motor é capaz de reduzir de maneira significativa o ruído gerado pelo motor turbofan. Desse ponto de partida, e utilizando-se de analogias da teoria eletromagnética da física, o motor é modelado como uma guia de onda cilíndrica. A equação para a propagação sonora na guia de onda cilíndrica neste modelo é deduzida a partir das equações de Navier-Stokes. Posteriormente, a equação diferencial para o campo de pressão na guia de onda é resolvida por meio de separação de variáveis, o que nos convida ao estudo das funções de Bessel e suas propriedades. Finalmente, de maneira a reproduzir o efeito das guias de onda HQ, uma analogia com fontes sonoras é empregada, o que mostra, por meio da teoria acústica e de equações diferenciais, o efeito do confinamento de energia causado pelas guias de onda HQ e seu papel em reduzir o ruído acústico que sai do motor turbofan. Apresenta-se uma conclusão para o estudo e melhorias para futuros trabalhos são sugeridas.

Palavras-chave: Aeroacústica. Física matemática. Guias de onda de Herschel-Quincke. Atenuação de ruído.

Table of Contents

List of Figures

List of Tables

Appendices

List of Symbols

Roman Letters

a	Turbofan inlet radius
B	Magnetic field
c	Wave speed, either for light or sound
E	Electric field
F	External forces
k	Wave number
M	Mach number
p'	Pressure fluctuations
R	Radius of the piston
t	Time
u_0	Vertical velocity of the piston
u_ω	Vertical velocity of the piston
v	Velocity of fluid molecules
V	Velocity of the airflow

List of Symbols

Greek Letters

β	Acoustic admittance of the surface, the reciprocal of the impedance
γ	Ratio of the resistance of the medium to the reactance of the baffle (piston)
η	Fluid viscosity
$\boldsymbol{\eta}$	General space coordinate
λ_m	m^{th} zero of the Bessel function of the first kind, order 1
ρ'	Density fluctuations
ρ_0	Density of the fluid
ω	Angular frequency

1 Introduction and Objectives

Despite technological improvement, turbofan engines are still a major source of acoustic noise in an aircraft, whose hazardous effects are felt most by people working and living in the vicinity of airports. More and more will aviation agencies create more stringent rules to assure that noise levels generated by aircraft are gradually reduced. Different passive technologies are currently used in an attempt to a greater reduction of sound noise, such as lobular mixers and liner technology, but there are inherent limitations that prevent them from achieving higher levels of noise reduction. In this context, the industry is open to new passive noise-attenuating technologies, as active control is a technology still under development. Herschel-Quincke waveguides could come as a new solution for noise attenuation mainly from the turbofan inlet.

In this study we study turbofan noise generation as a whole and present some of the technologies currently used to reduce noise generation. Then Herschel-Quincke waveguides are first introduced and experimental results concerning its use in a study by Burdisso and Smith are shown. The study demonstrates the potential of the Herschel-Quincke waveguides as a noise attenuator device, and with this motivation, we initiate a theoretical study of the noise propagation at the turbofan engine, here modelled as a cylindrical waveguide. After finding an expression for the pressure field inside the turbofan, we attempt to create a theoretical model for the Herschel-Quincke waveguides, and based on the theory of sound sources and Green's functions, we find an expression for noise attenuation of the pressure field inside the turbofan engine.

The main objective of this work is to enhance the theoretical understanding of waveguides in an aeroacoustic setting with practical relevance, by use of the mathematical tools and their meaning in the expressions. That is one reason why the deductions and mathematical passages are very detailed. In this way it is possible to help the reader to have a thorough understanding of the concepts involved and motivate him to advance in this study. As computational tools are today widely available, a further step in this work would be to do a numerical simulation of the effect of the Herschel-Quincke waveguides in a turbofan engine and compare the results with experiments.

2 Turbofan engine noise and the Herschel-Quincke technique

2.1 Turbofan engine noise

Turbofan engines are the preference choice of aircraft manufacturers due to their advantages over other engine types, such as the turbojet and the turboprop. The turbojet is very inefficient, as all the air that is admitted to the engine is also accelerated in the combustion process. When the accelerated mass of air leaves the engine, it interacts with the atmosphere, causing pressure changes that lead to big energy losses and a lot of acoustic noise. The turboprop is a more efficient engine but it presents limitations in the cruise speed aircraft can develop, what makes this aircraft more suitable for regional aviation. Thus, the turbofan is the best choice for aircraft engine in most situations. Fig. 1 presents a depiction of a Pratt & Whitney F100 turbofan engine. Air is admitted through the inlet, later being propelled by the fan. Then part of the air passes through the core, while the other part enters in a chamber around the core, also called bypass. The air which passes through the core is heated and later mixed with the bypass air. The ratio between the air mass which passes around the core and the mass which passes through the core is called *bypass ratio*. The fact that air passes through two different chambers account for less energy losses for this type of engine, what in turn also leads to less acoustic noise emissions. These are some reasons the turbofan engine is a premier choice for manufacturers [1].

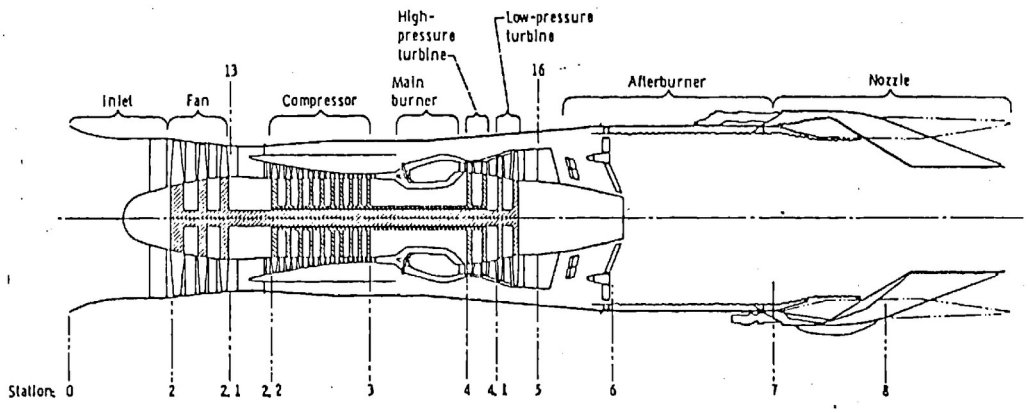

Fig2.4: Schematic of the F100 Engine (from [1]).

Fig. 1: Pratt & Whitney F100 - example of a turbofan engine
Source: [2]

There are a variety of processes which generate noise in the operation of a turbofan engine. Usually noise in a turbofan is divided into two categories: broadband noise of aerodynamic origin and line spectrum noise of multiples of blade-passage frequency (also called tonal noise). Broadband noise is usually generated by vortex shedding, boundary layer turbulence, interaction between the blade pressure fields, wall boundary layer, among others. As for the line spectrum noise, the sources of these type of noise involve steady aerodynamic blade loading and blade thickness and also vortex shedding, transient aerodynamic loading variations due to turbulence, and blade vibration. In essence, many of the sound-generating processes for the latter type of noise can be attributed to the interaction between the rotor blades and the stator vanes [3], [4]. The exact mathematical modelling of those sound-generating processes for each of the sources can be quite difficult and will not be attempted at this work.

2.2 Noise abatement in turbofan engines

Usually sound produced by turbofan engines can be divided into two categories pertaining to the location of the sources: at the inlet and the outlet. For the latter, also called exhaust jet noise, possible technologies for noise reduction are: jet velocity reduction, which can be achieved by increasing the bypass ratio (though this can have a harmful effect in increasing tonal noise), the use of lobular mixers and the use of chevron and sawtooth nozzles. Increasing the bypass ratio is an interesting solution because enables the maintenance of thrust for the aircraft engine while increasing fuel efficiency and reducing noise [5]. Lobular mixers are important because they help impart linear momentum to the bypass air, in a way that increases efficiency and reduces noise [1]. As for the nozzles in chevron an sawtooth geometries, they help can control the shear layer by generating turbulence, which delays separation and avoids bigger generation of noise.

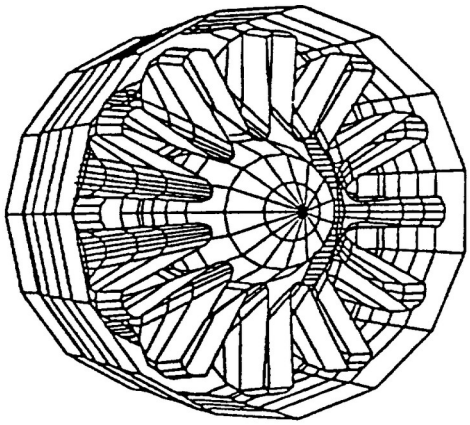

Figure 11 Three Dimensional Display of JT8D-209 Mixer Geometry

Fig. 2: Lobular mixer of a Pratt & Whitney JT8D-209 turbofan engine
Source: [6]

FIG. 1

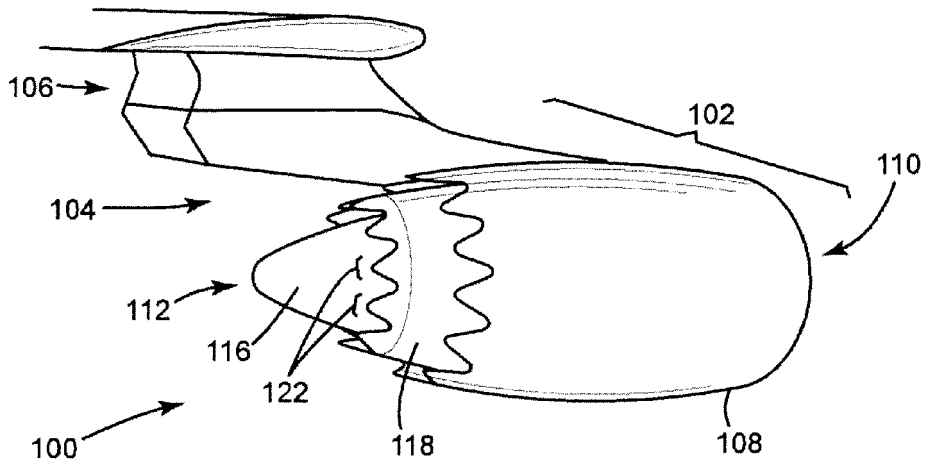

Fig. 3: Chevron nozzle of a turbofan engine
Source: [7]

In regard to the engine inlet, several improvements with the goal of reducing noise emission are possible. The geometry and the number of the fan blades and the rotor vanes can be changed for a configuration capable to reduce mainly tonal noise. Clearly, these changes could modify the aerodynamic flow inside the engine, generating noise from undesired side effects. A research field that is gaining traction over the last years is active noise control. A computational model is made, consisted of different acoustic and engine performance variables. Thus, the physical variables inside the engine are measured and the control system is capable to find optimal configurations for the engine performance through actuators while reducing acoustic noise [8]. Despite its potential, active noise control is yet to reach maturity and therefore is not utilised in industry in a broad scale [4]. Reference [7] is an example of the development of this technology for a more concrete use.

2.2.1 Liner technology

As opposed to active control, liner technology consists of passive sound absorbers, made of porous material, which can be divided in two types. Absorber liners from material like foam or expanded polystyrene causes the air inside the pores to vibrate. The relative motion between this air and the skeleton dissipates sound energy into heat by friction. There is also an additional energy loss due to the heat exchange between the heated compressed air and the solid skeleton. This means that this kind of liners dissipate energy irrespective of the pressure frequency and are appropriate for broadband noise attenuation [4], [9]. Conversely, resonant liners, which appear in perforated or honeycomb panels with a cavity act like a Helmholtz resonator, attenuating better pressure waves with the same frequency as the resonant cavity, thus being appropriate for abatement of noise of a specific frequency. They prove very useful in reducing the tonal frequency of blade passage, for instance, but apart from this, are inefficient in lowering broadband noise, while occupying a considerable volume inside the engine [4], [9]. Liner technology is undoubtedly useful, but it has its limitations, because liners have a very well-defined structure and there is not much room for improvements or new configurations, making their overuse not feasible for efficient applications. In this context, new noise-reducing passive technologies are certainly welcome, and that is a very good motivation to introduce the concept of Herschel-Quincke waveguides.

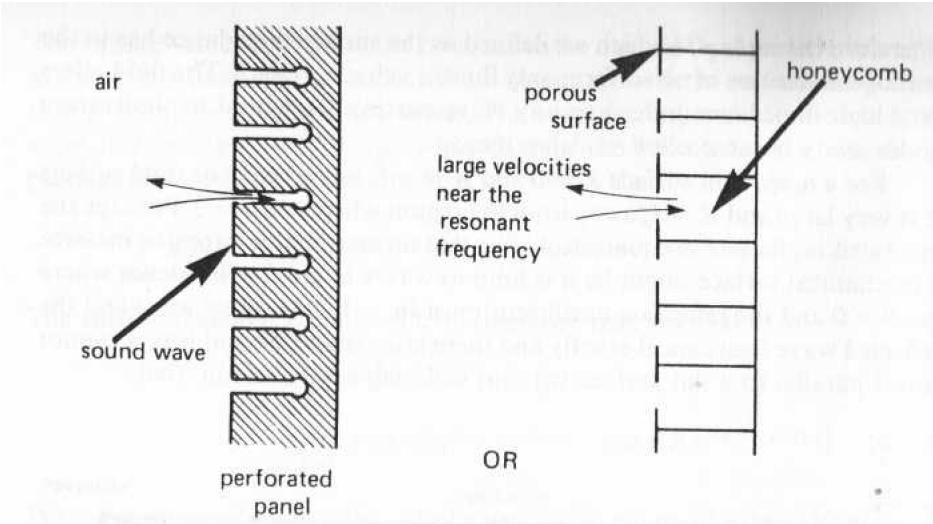

Fig. 4.9 — Types of sound absorbers.

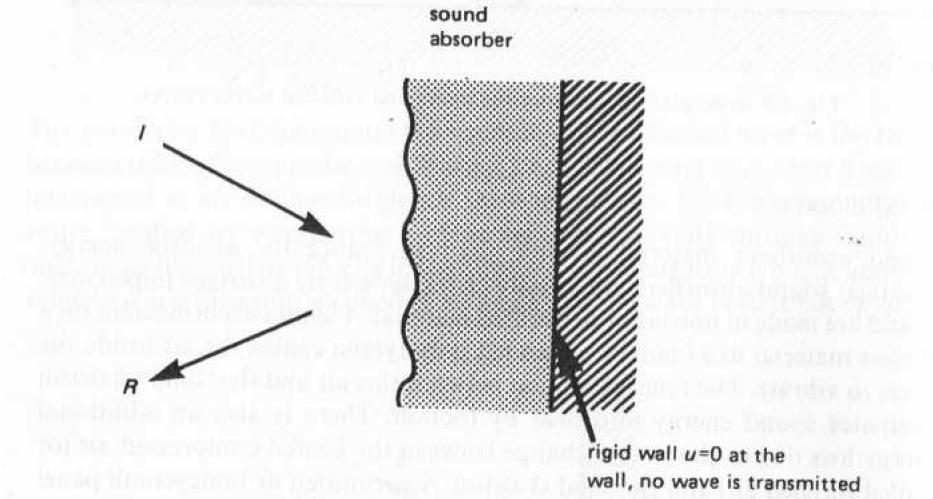

Fig. 4.10 — A sound absorber on a rigid wall.

Fig. 4: Types of liner: absorber and resonant
Source: [9]

2.3 The Herschel-Quincke technique

2.3.1 Definition and history

A Herschel-Quincke waveguide (or tube, according to several references on the topic)[1] is a tube that has one of its openings attached to a main tube, and the other opening also attached to the main tube, but in a different position from the first opening. The line linking the first and the second openings of the tube in most cases is parallel to the axis of the main tube. It can be said that the tube will have the shape of a circumference arc when cut longitudinally. And the shape of its transversal section is a circle. Fig. 5 presents an example of a Herschel-Quincke (HQ) waveguide:

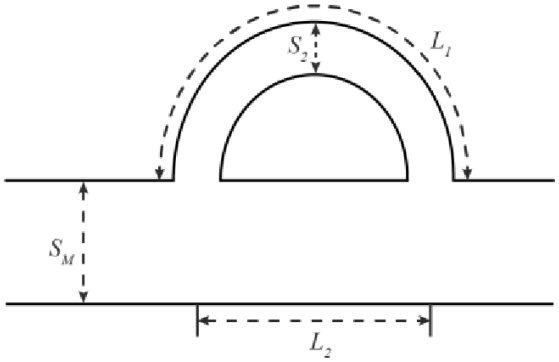

Fig. 5: General example of a HQ waveguide
Source: adapted from [10]

Next is shown this HQ waveguide concept applied to the inlet of a turbofan engine:

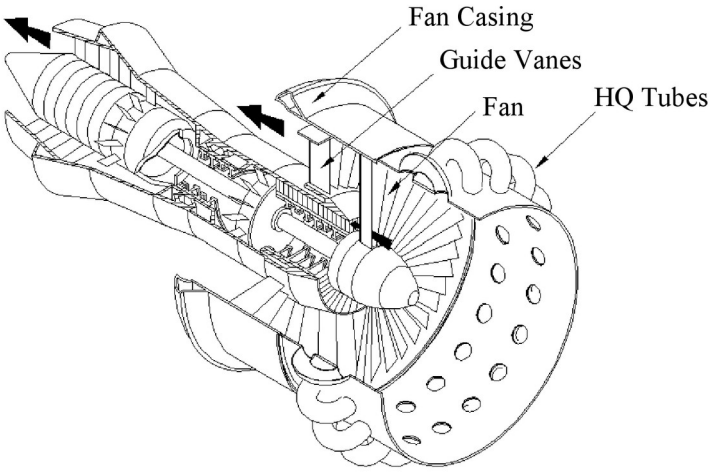

Fig. 6: HQ waveguides applied to the inlet of a turbofan engine
Source: [4]

[1] The fact that we call it a Herschel-Quincke waveguide or tube is just a matter of nomenclature. To be consistent with the experimental reference which will be presented in the next subsection, we use the term “waveguide”.

The entire circumference of the inlet of the engine is permeated by several HQ waveguides, each parallel to the other, to assure noise attenuation in all of the circumferential coordinate; it could be that some modes would not be affected by the HQ waveguides if they were not distributed in all of the circumference of the inlet. Also, this distribution guarantees symmetry in the noise abatement effects. That is one reason why all waveguides have the same dimensions.

The Herschel-Quincke waveguide owes its name to the scientists who proposed this guide design and made experiments with light (electromagnetic waves) in the 19th century. The HQ waveguide has been studied by various authors, but received little attention as a sound attenuation device until the late 1970s [11]. In the 1990s, Selamet, Dickey and Novak theoretically and experimentally investigated the HQ waveguide without flow and without end reflection, developed a general expression for transmission loss and presented a non-linear one-dimensional finite-difference model [11], [12]. At the outset of the 20th century, Burdisso and Smith [13] developed an extensive experimental study on noise attenuation in a turbofan engine with an innovative implementation of the Herschel-Quincke waveguides which will be the subject of subsection 2.4.

2.3.2 Geometrical characteristics and wave interference

The Herschel-Quincke waveguide clearly has a very definite set of geometrical features, which are responsible for the sound-attenuating mechanisms. These characteristics have been studied since the inception of the concept. Herschel, still in the 19th century, predicted that the cancellation of tones would occur when the path length difference between the recombined signals was $(2m+1)(\lambda/2)$, with λ being the wavelength and m an integer. Later, in 1866, Quincke experimentally validated that Herschel's system did effectively cancel sound. George W. Stewart, in 1928, verified that cancellation does occur when the path length difference is $(2m+1)(\lambda/2)$, but also when the path length difference is $m\lambda$, with limited attenuation at other transitional frequencies [4].

In addition to the difference between the paths of the sound waves, there are theoretical models which take into consideration other geometrical variables such as the dia-

meter of the Herschel-Quincke waveguides, their length and also the distance between the two openings of a certain tube.

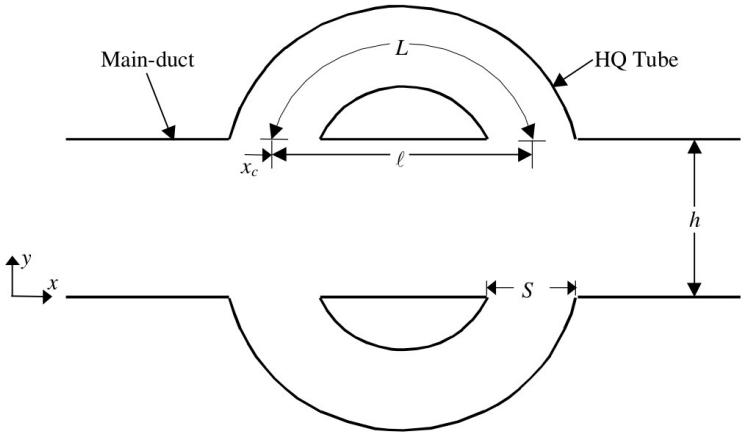

Fig. 7: Herschel-Quincke waveguide modelling concept
Source: [14]

Brady's model, presented in Fig. 7, is bidimensional and determines the equations for the pressure field at the HQ waveguide and the main waveguide separately, later coupling both equations. When the equation for the transmitted pressure field is shown, it is seen that it depends on the diameter of the HQ waveguide S, its length L and the distance between the openings of two tubes l. This model also presents a way to predict the frequency of maximum attenuation for individual modes, which will depend on a transcendental equation that features the same geometrical variables S, L and l. Therefore, not only the geometry of the tube influences the resulting pressure field, but it also presents a way to modulate the resonance frequencies that can better attenuate noise from the turbofan engine.

Because of this, an interesting extension of HQ tube design for the suppression of higher-order modes might include active control of an aspect of tube geometry in order to attain optimum attenuation of sound at a range of frequencies. For instance, in some noise control applications, it may be feasible to adjust the length of the HQ tube [14].

2.4 Experimental data on Herschel-Quincke waveguides

2.4.1 Motivation

A typical fan acoustic spectrum includes a broadband noise level and tones at the fan blade passage frequency (BPF) and its harmonics. These tones are often at least $10-15\ dB$ above the broadband level. Future ultra high bypass ratio turbofan engines (ratios of up to 10) will have an even greater fan tonal noise component at lower frequencies. The shorter inlet ducts relative to the size of the fan and the lower BPFs expected for these engines will make traditional passive liner technology less effective for attenuating the fan tones [13]. In this context, new noise-reducing passive technologies such as the Herschel-Quincke waveguides can provide better results while active control technology does not reach widespread use.

2.4.2 The experiment set-up

In the study carried in reference [13], Burdisso and Smith implemented an array of HQ waveguides around the circumference of the Pratt & Whitney JT15D turbofan engine inlet. This engine has been used extensively for research in passive and active noise control methods applied to turbofan engines. It is a twin spool turbofan engine with a full length bypass duct and a maximum bypass ratio of 2.7 . The engine is equipped with an inlet inflow control device (ICD). Its purpose is to minimize the spurious effects of ground testing on acoustic measurements by breaking up incoming vortices. The maximum diameter of the ICD is 2.1 times the engine inlet diameter. Finally, the engine is mounted in a test cell, which is divided into two chambers by a transmission loss partition. The forward chamber is anechoic to simulate free field conditions, where only the inlet is inside. This serves the purpose of isolating the radiation of the inlet from the aft and jet noise radiation. One wall of the anechoic chamber is open to the atmosphere for engine intake air as depicted in Fig. 8 [13].

In these experiments, one and two arrays of HQ tubes are mounted circumferentially around the cylindrical perforated mesh inlet of the turbofan jet engine. For clarity, the inlet configured with one and two arrays of HQ tubes will be denoted as the 1AHQ and 2AHQ inlets, respectively. The surface area of the inlet section where the tubes were not attached was configured as a rigid wall. All of the tubes are axially-oriented (i.e., extend parallel to the engine axis) as shown in the configuration schematic in Fig.

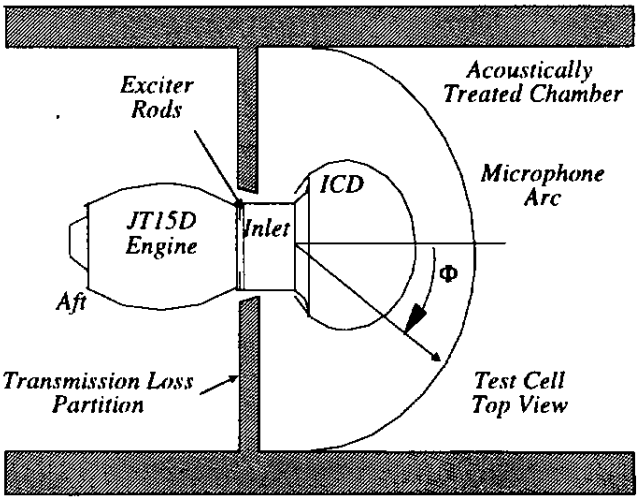

Fig. 8: Depiction of turbofan engine test cell
Source: [13]

6. Figs. 9 and 10 show pictures of the engine inlet configured as a hard-wall and with two arrays of HQ tubes, respectively. In Fig. the bottom panel is left off so that the mesh screen cylinder is visible [13].

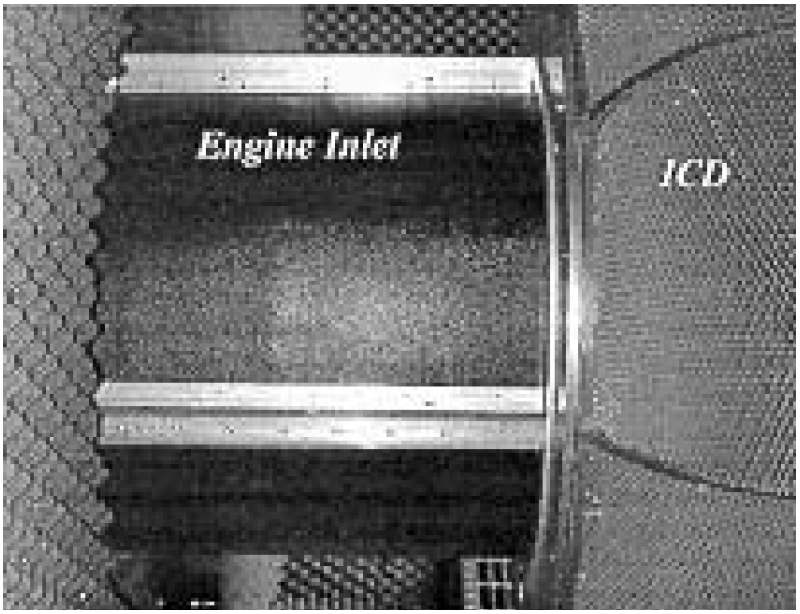

Fig. 9: JT15D inlet configured as a hard wall
Source: [13]

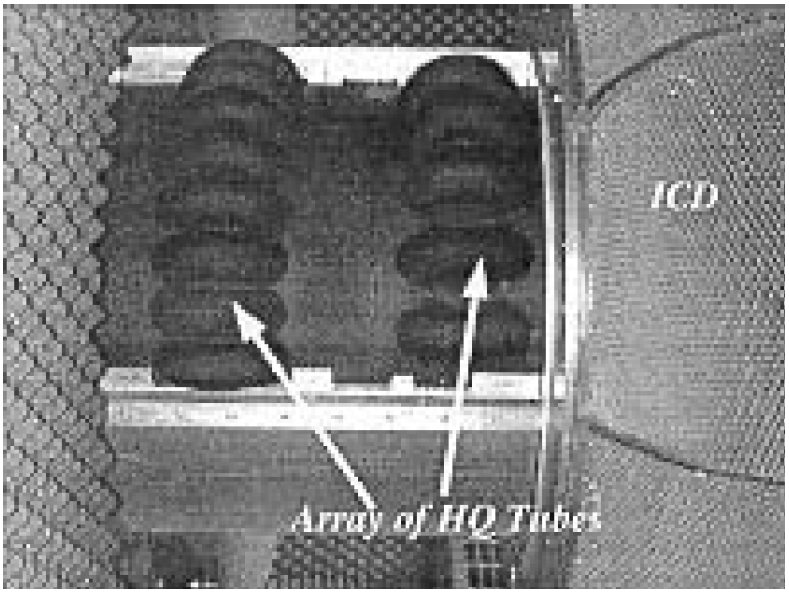

Fig. 10: JT15D inlet configured with two arrays of HQ tubes
Source: [13]

Two HQ tube configurations are investigated as shown in Fig. 11. The first configuration consists of a single array of 20 HQ tubs (1AHQ inlet) while the second is configured with two arrays of HQ tubes with 20 and 16 tubes, respectively (2AHQ inlet) [13].

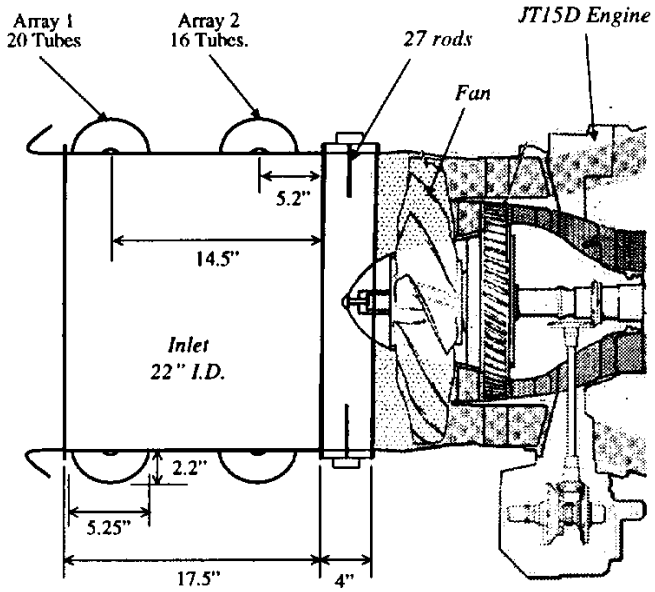

Fig. 11: Configurations of one and two arrays of HQ tubes
Source: [13]

2.4.3 Experimental results

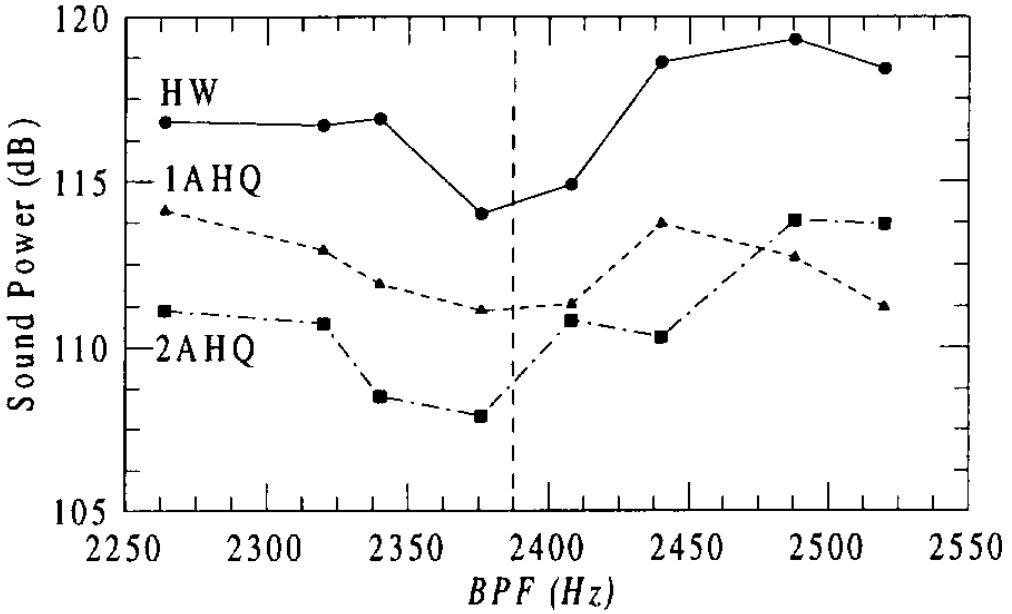

Fig. 12: Acoustic power at the BPF tone, sector from 0° to 90°
Source: [13]

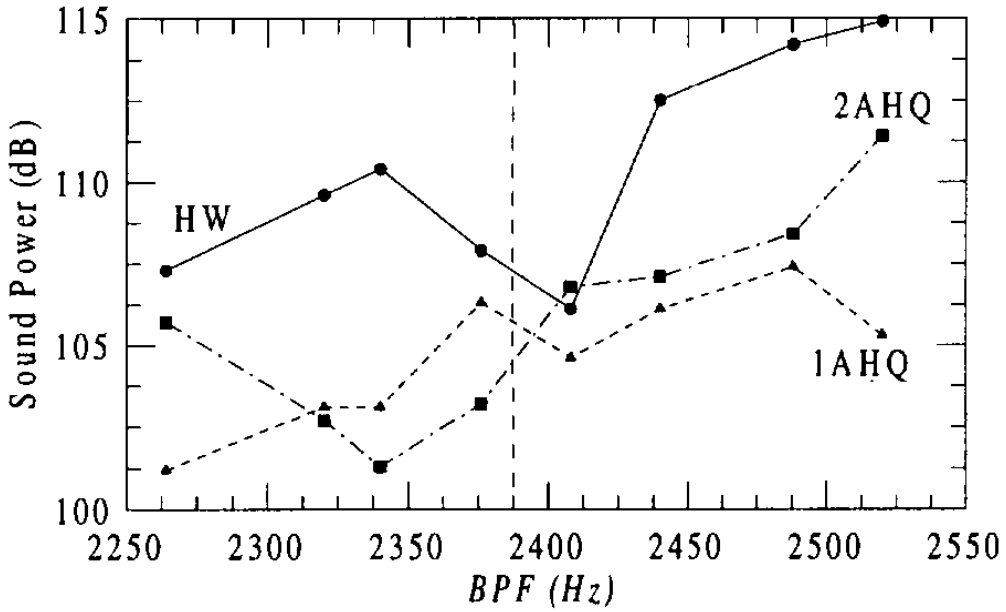

Fig. 13: Acoustic power at the BPF tone, sector from 50° to 90°
Source: [13]

BPF (Hz)	Sector 0° - 90°		Sector 50° - 90°	
	1 Array	2 Arrays	1 Array	2 Arrays
2340	5.0	8.6	7.3	9.5
2440	4.8	8.2	6.5	5.2

Tab. 1: Power Level Reduction at BPF tone
Source: [13]

Figs. 12 and 13 show the acoustic power, in decibels, at the BPF tone for the sectors 0° to 90° and 50° to 90° , respectively. It is possible to see that the HQ waveguide has a positive effect on noise reduction, as the results with the configuration 2AHQ have indeed a lesser level of noise power, noticeably lower around the BPF frequency tone.

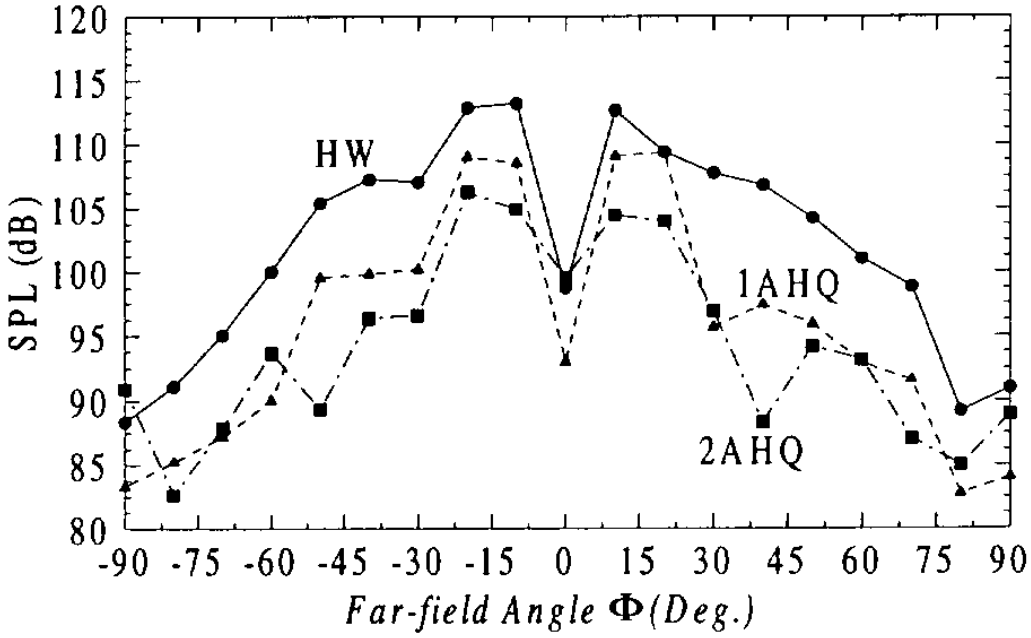

Fig. 14: Sound pressure directivity at BPF tone, BPF=2340 Hz
Source: [13]

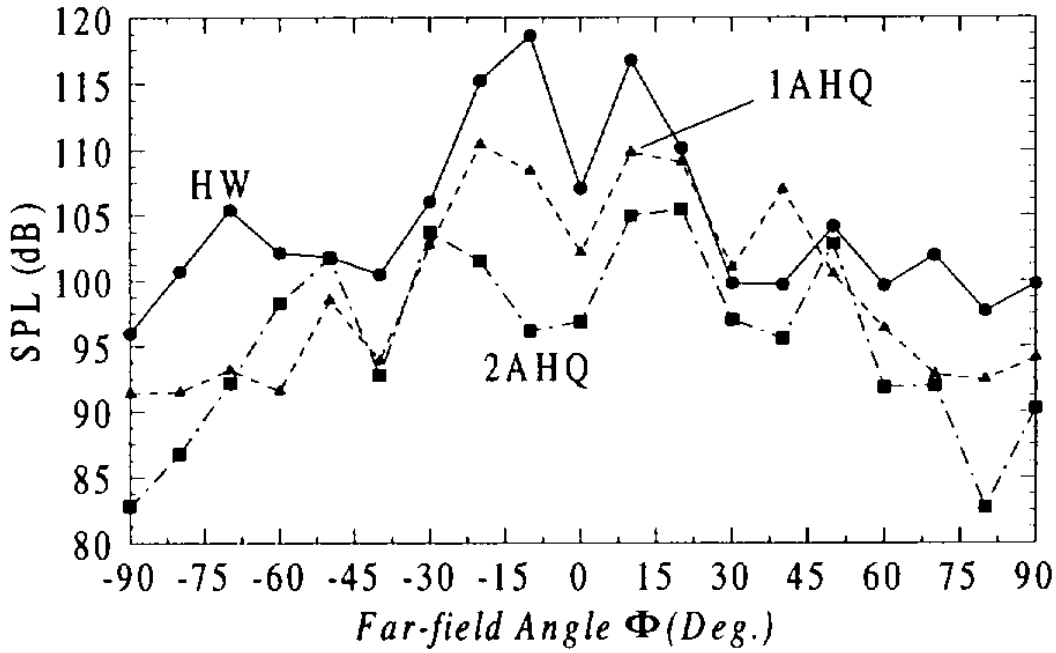

Fig. 15: Sound pressure directivity at BPF tone, BPF=2440 Hz
Source: [13]

As for Figs. 14 and 15, the directivity of the sound noise is shown for different values of the BPF frequency. It is possible to see an accentuated noise reduction around the angle $0°$, which is not the case for the angle $\pm 15°$. Then a progressive reduction on SPL is noticed, and the lowest values for SPL are seen around the angle $\pm 90°$. Again, the best results are obtained with the 2AHQ configuration, and the 1AHQ configuration is better than the hard wall configuration for noise reduction purposes.

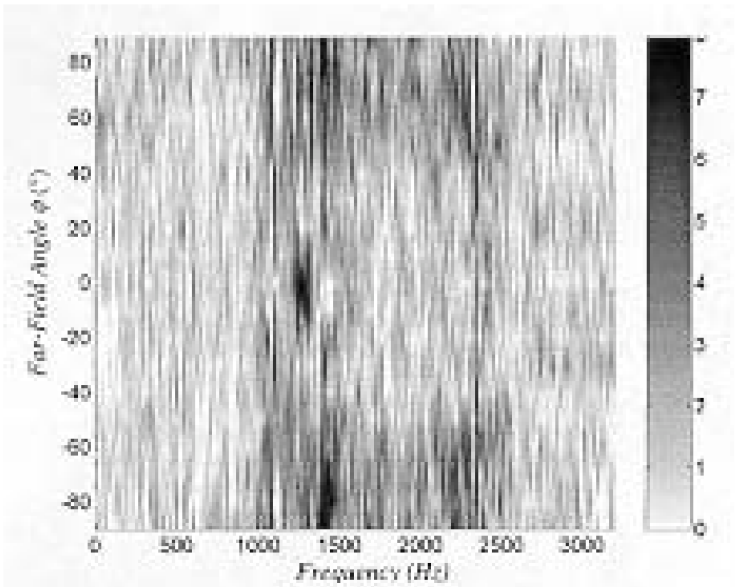

Fig. 16: SPL reduction vs . frequency and far-field angle for 1AHQ inlet
Source: [13]

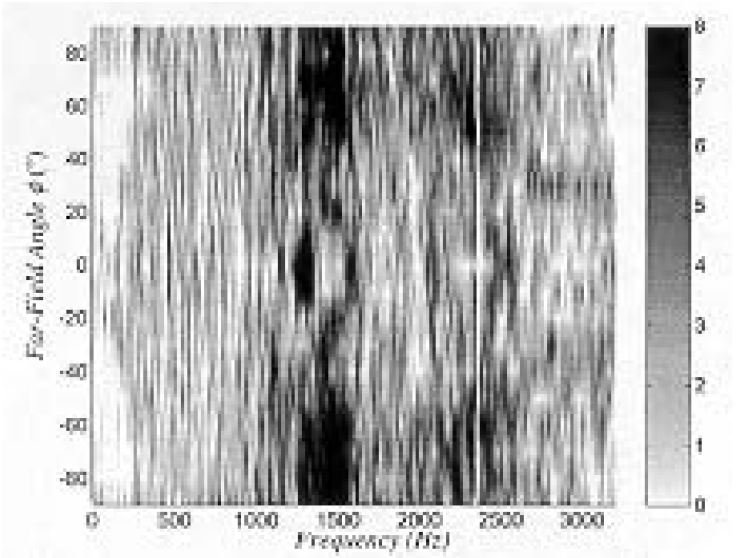

Fig. 17: SPL reduction vs . frequency and far-field angle for 2AHQ inlet
Source: [13]

Now, Figs. 16 and 17 show that for both configurations of the Herschel-Quincke arrays of waveguides, there is indeed a broadband noise reduction, because it can be seen that for all frequencies, there is some SPL reduction, but it specially occurs around the BPF frequencies, which happen between $1000-1500\,Hz$ and $2000-2500\,Hz$. In this case, there is tonal noise reduction at the BPF.

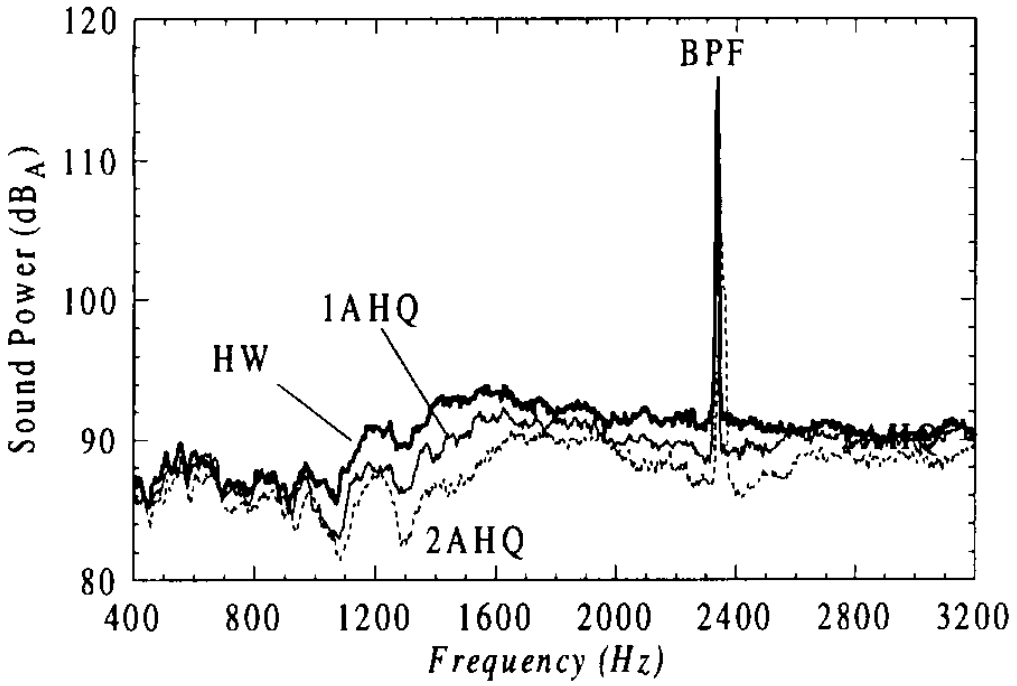

Fig. 18: Acoustic power spectra for the HW, 1AHQ, 2AHQ inlets for sector 0° - 90°
Source: [13]

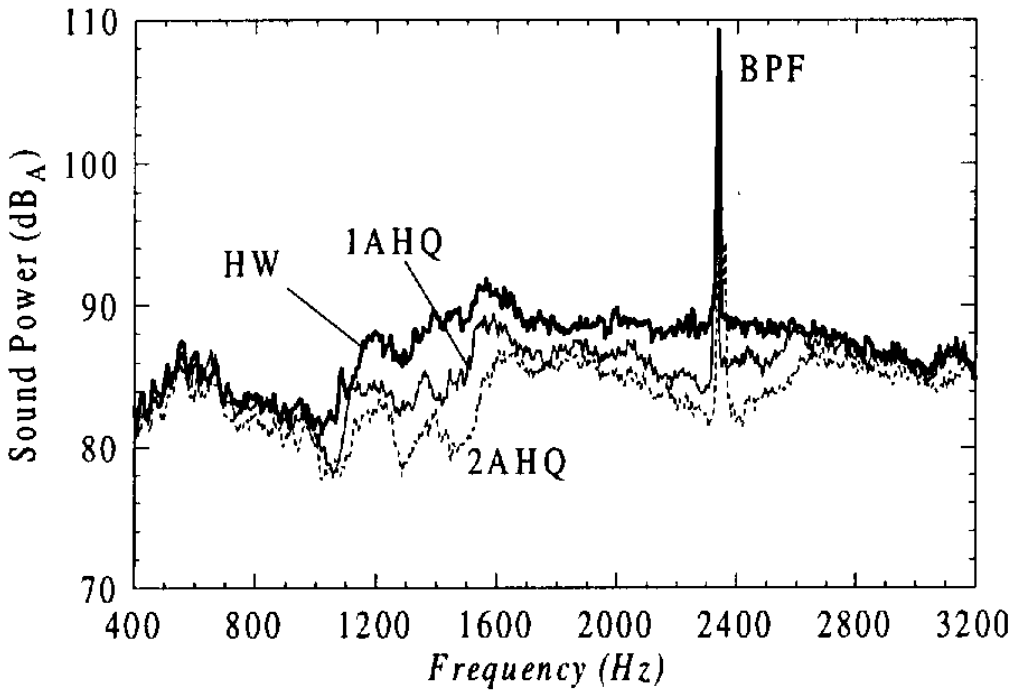

Fig. 19: Acoustic power spectra for the HW, 1AHQ, 2AHQ inlets for sector 50° - 90°
Source: [13]

Combination of Broadband and BPF Tone Reductions	***Overall Power Reduction (dB)***	
	1AHQ	***2AHQ***
Actual Broaband Red. + Actual BPF tone Red.	2.7	4.6
Complete removal of BPF tone only	2.6	2.6
Actual Broadband Red. + Total BPF tone Red.	4.1	5.6

Tab. 2: Overall Power Level Reductions – 0° - 90° Sector
Source: [13]

Combination of Broadband and BPF Tone Reductions	***Overall Power Reduction (dB)***	
	1AHQ	***2AHQ***
Actual Broaband Red. + Actual BPF tone Red.	2.8	4.4
Complete removal of BPF tone only	1.4	1.4
Actual Broadband Red. + Total BPF tone Red.	3.2	4.8

Tab. 3: Overall Power Level Reductions – 50° - 90° Sector
Source: [13]

Figs. 18 and 19 make very clear that the tonal noise at the BPF generates a considerably louder tone, which is clearly felt by people who live near airport zones. It also shows the potential of the Herschel-Quincke waveguide in reducing the pressure level for a spectra of frequency values.

Based on the experiment set-up and our knowledge of waves, we could try to elaborate an explanation on wave attenuation referring only to the geometrical disposition of the Herschel-Quincke waveguide and the conditions of the experiment. By reading the experiment paper [13], we find that at that condition the sound speed was $c = 42.5 / 0.12 = 354.17\ m/s$. We also know that the HQ waveguides were designed mainly to attenuate sound at the $2320\,Hz$ frequency. This enables us to find the wavelength of those sound waves in such a scenario, which is $\lambda = 0.15266\ m$. In subsection 2.3.2 we discovered that destructive interference occurs for $(2m+1)(\lambda / 2)$ and $m\lambda$. This is equivalent to $(2m+1) \times 0.076329\ m$ and $m \times 0.15266\ m$, while the path difference between a wave that goes inside the HQ waveguide and other that stays in the main cylindrical waveguide is of the order of $0.01\ m$. Thus, in a first inspection, the phenomenon of sound attenuation could not be explained by destructive interference due to path difference. The distance between the two arrays of tubes is approximately $0.1683\ m$, which is close to λ, but a relation between the two amounts based in wave interference is not immediate.

Therefore, we can conclude through this experimental study that a Herschel-Quincke waveguide mounted at the inlet of a turbofan engine is able to present satisfactory results in the reduction of the sound power level for different frequencies. When this array of waveguides is adjusted accordingly for the geometry of the engine inlet, it can also contribute to the reduction of sound tones for the blade passage frequency, which is a major source of noise for people and affects considerably the Effective Perceived Noise Level (EPNL) scale. To better understand how a Herschel-Quincke waveguide can be useful at the inlet of turbofan engines, it can be useful to study how it attenuates noise from a theoretical standpoint; this way, we might gain insights that will enable other researchers and the industry to provide effective solutions for the aircraft engine noise problem. This theoretical study will be done in the next sections.

3 Waveguides

3.1 Electromagnetic waveguides

Waveguides are structures which confine electromagnetic waves, enabling the propagation of this wave in a certain direction. They were particularly utilised during the 1960s, on the radar age, because of their properties to propagate waves from one location to another with minimal energy loss [15]. Dealing with electromagnetic waves, we can assume the material which makes up the waveguide is a perfect conductor, what, in practical applications, would mean that it is made of a metal. In order to show the parallels between the electromagnetic theory of waveguides and the acoustic one, the equations for the electromagnetic waveguide are derived in some depth.

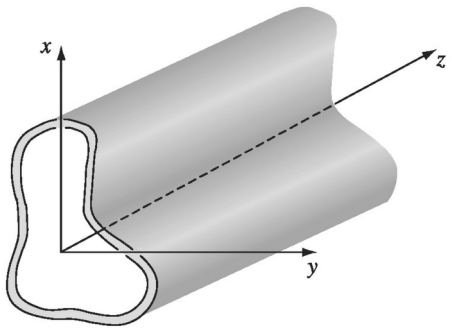

FIGURE 9.23

Fig. 20: Example of a waveguide
Source: [16]

The boundary conditions for the propagation of the electromagnetic waves in the waveguide are as follows:

$$\begin{aligned} (i)\ \ \boldsymbol{E}^{\parallel} &= 0, \\ (ii)\ \ \boldsymbol{B}^{\perp} &= 0. \end{aligned} \tag{1}$$

The conditions specified by equations (1) are only valid on the inner surface of the conductor; there is not, in principle, any constraint for the values of the fields on the hollow space inside the guide. Because we want to find monochromatic waves that propagate down the tube, the electric and magnetic fields will have the generic form [16]:

$$\begin{aligned} (i)\ \ \widetilde{\boldsymbol{E}}(x,y,z,t) &= \widetilde{\boldsymbol{E}}_0(x,y)e^{i(kz-\omega t)}, \\ (ii)\ \ \widetilde{\boldsymbol{B}}(x,y,z,t) &= \widetilde{\boldsymbol{B}}_0(x,y)e^{i(kz-\omega t)}. \end{aligned} \tag{2}$$

The electric and magnetic fields must, evidently, obey Maxwell's equations, in the interior of the waveguide [16]:

$$\begin{aligned} (i)\ \nabla\cdot\boldsymbol{E} &= 0, \quad (iii)\ \nabla\times\boldsymbol{E} = -\frac{\partial \boldsymbol{B}}{\partial t}, \\ (ii)\ \nabla\cdot\boldsymbol{B} &= 0, \quad (iv)\ \nabla\times\boldsymbol{B} = \frac{1}{c^2}\frac{\partial \boldsymbol{E}}{\partial t}. \end{aligned} \tag{3}$$

To find a solution to equations (3), subject to the boundary conditions specified in (1), it is necessary to propose electric and magnetic fields with vector components in the three axes[2]. By applying this three-vector field form in the equations, and after quite a lot of algebraic work, we find the following differential equations [16]:

$$\begin{aligned} \left[\frac{\partial^2}{\partial x^2}+\frac{\partial^2}{\partial y^2}+(\omega/c)^2-k^2\right]E_z &= 0, \\ \left[\frac{\partial^2}{\partial x^2}+\frac{\partial^2}{\partial y^2}+(\omega/c)^2-k^2\right]B_z &= 0. \end{aligned} \tag{4}$$

When $E_z=0$, these waves are called TE ("transverse electric"), while for $B_z=0$, they are called TM ("transverse magnetic"). We will now focus on the TE case. But the method to solve each of them is the same. If we have $E_z=0$, we still need to solve the equation for B_z , which is a function of two variables, x and y . In this section, for simplicity, we will solve the equations for a rectangular waveguide depicted in Fig. 21.

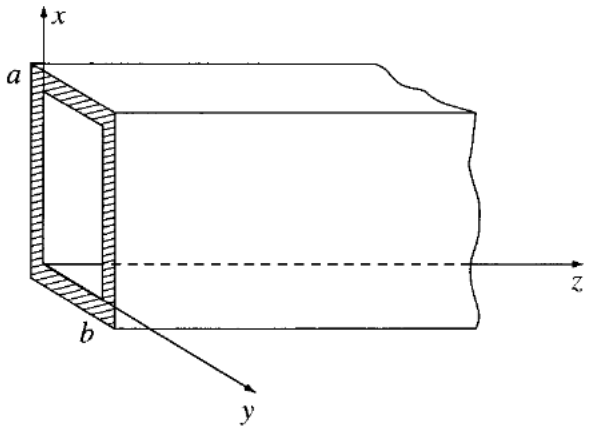

Figure 9.24

Fig. 21: Depiction of a rectangular waveguide
Source: [16]

[2] This is due to the nature of the problem, as we deal with confined waves. In non-confined cases it would be possible to have transverse waves.

The most common way to solve this equation, one of equations (4), is by separation of variables:

$$B_z(x,y) = X(x)Y(y) \tag{5}$$

Finally, the solution for the magnetic field in this case is:

$$B_z = B_0 \cos(m\pi x/a)\cos(n\pi y/b) \tag{6}$$

With m and n non-negative integers. The other components of the magnetic and electric fields can also be obtained, but their formulas will be here omitted. For more information on the subject, see [16]. And the wave number is given by:

$$k = \sqrt{(\omega/c)^2 - \pi^2[(m/a)^2 + (n/b)^2]} \tag{7}$$

If this wave number is complex, it means that instead of a wave, there would be exponentially decreasing fields. When this happens, we have the following situation:

$$\omega < \omega_{mn} \tag{8}$$

With ω_{mn} defined as:

$$\omega_{mn} \equiv c\pi\sqrt{(m/a)^2 + (n/b)^2}. \tag{9}$$

ω_{mn} is called the cutoff frequency, because waves with lesser frequencies would not propagate. Clearly, ω_{mn} depends on the mode, that is, the integers m and n. The lowest cutoff frequency for a given waveguide occurs for the mode TE_{10}:

$$\omega_{10} = c\pi/a \tag{10}$$

Lower frequencies cannot propagate in such a waveguide under no circumstances [16].

3.2 Modelling of the turbofan inlet as an acoustic waveguide

By the same token, we can consider a turbofan engine, a cylindrical structure with an enclosed geometry, a waveguide. Sound, as well as electromagnetic waves, is a kind of wave, which obeys the wave equation and because of this, similar results from the theory of waveguides can be obtained even if the physical equations governing the phenomena are in their appearance different[3].

[3] Electromagnetism and fluid dynamics share a lot of mathematical similarities, which can be quite useful in theoretical development, like here. But one cannot deny the fact that, in the electromagnetic derivation of waveguides, we started from Maxwell's equations, and here, we will start from Navier-Stokes equations.

It is important to note that in this development, we will consider sound propagation in a turbofan engine, here modelled as a waveguide, without a mathematical source of sound. But this description can be valuable notwithstanding, because, in the words of [17], "*In the sound field, q must be zero because sound waves satisfy the homogeneous wave equation. The source region, V, where $q(\boldsymbol{x},t)$ is non-zero, is thus clearly separated from the sound field where must vanish. We have said that this definition of a sound source is somewhat arbitrary, and indeed knowledge of the sound field is not sufficient to uniquely determine the source.*"

This means that the sound-generating processes which take place inside the turbofan, such as rotor-stator interaction, boundary layer phenomena, among others, do not need to be considered if we are only interested in sound propagation, because sound waves satisfy the homogeneous wave equation. Therefore, it can be understood that studying only sound propagation without a source could describe an adequate view of sound propagation inside the turbofan engine. But the extent to which this assumption can provide an accurate evaluation of the sound field inside the turbofan engine is debatable, because we could reasonably assume that all of the engine is inside the source region V. Nonetheless, as the sound-generating processes inside the engine can be quite complicated to model, studying the sound propagation by itself, without a source, can still give us some useful perspectives on acoustic properties of the turbofan, while being a more tractable problem than modelling each sound-generating process inside the engine.

For the treatment of the turbofan engine as an acoustic waveguide, we neglect the reflections at the open end of the inlet and on the fan. To do so we consider the turbofan engine, in its geometry, a hard-walled cylindrical duct with infinite length. Fig. 22 presents the duct, with radius a, through which a uniform air flow with velocity $\boldsymbol{V}$ passes. This velocity field is parallel to the z axis. Sound propagation is in the same direction as the z axis [4].

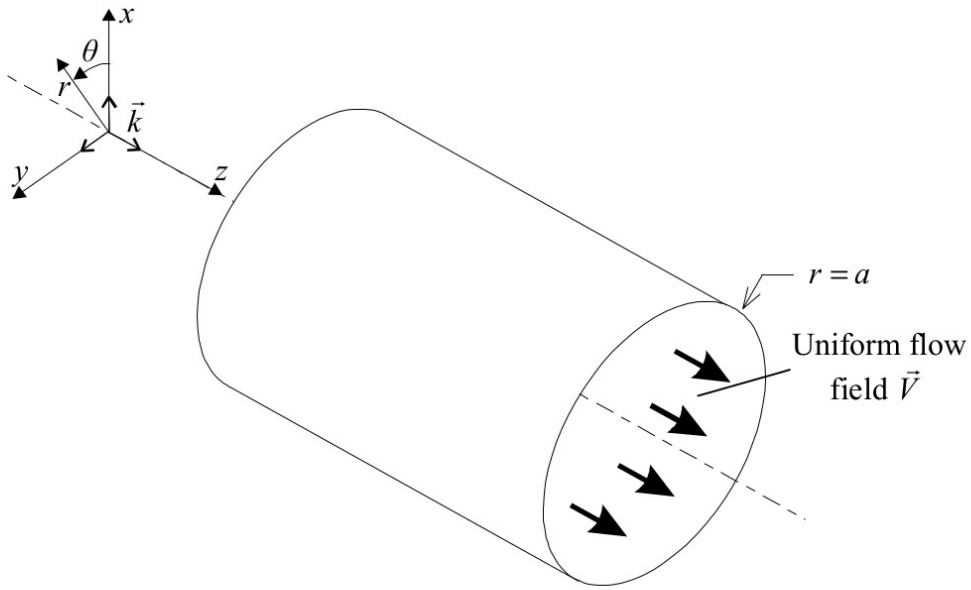

Figure 2-2: Model of the infinite cylindrical duct with flow.

Fig. 22: Turbofan model as an infinite cylindrical waveguide
Source: [4]

The generic form of the acoustic wave equation in a moving media is as follows [18]:

$$\frac{1}{c^2}\left(\frac{\partial}{\partial t}+\boldsymbol{V}\cdot\nabla\right)^2 p' = \nabla^2 p' \tag{11}$$

We are going to prove this equation (11) from Navier-Stokes equations in the next section. This is something that neither [4] nor [18] do.

3.3 Deduction of the acoustic wave equation in moving media from Navier-Stokes equations

Navier-Stokes equations are differential equations governing the motion of compressible, Newtonian fluid. They arise from conservation laws, namely, the conservation of mass, the conservation of momentum and the conservation of energy. For the purposes of this proof we will only need conservation of mass and momentum. The continuity equation, the equation for conservation of mass, is written as:

$$\frac{\partial \rho'}{\partial t}+\rho_0 \nabla\cdot\boldsymbol{v} = 0 \tag{12}$$

In (12) we are only considering first-order terms, and neglecting those of lower magnitude [19]. Following that equation we have the general form for the conservation of momentum, which is also Newton's second law [20]:

$$\rho\left(\frac{\partial}{\partial t}+\boldsymbol{v}\cdot\nabla\right)\boldsymbol{v} \;=\; -\nabla p+\eta\left[\nabla^2\boldsymbol{v}+\frac{1}{3}\nabla(\nabla\cdot\boldsymbol{v})\right]+\boldsymbol{F} \tag{13}$$

In its most complete form, viscosity effects would need to be considered, but here we neglect them. Smaller terms are also neglected, and thus the first-order equation for conservation of momentum is:

$$\rho_0\frac{\partial\boldsymbol{v}}{\partial t} \;=\; -\nabla p' \tag{14}$$

Now, if the fluid is moving with a velocity field, whose magnitude is $\boldsymbol{V}$, the continuity and conservation of momentum equations are, in relation to the laboratory frame [18]:

$$\begin{aligned}&(i)\quad \left(\frac{\partial}{\partial t}+\boldsymbol{V}\cdot\nabla\right)\rho'+\rho_0\nabla\cdot\boldsymbol{v} \;=\; 0\\ &(ii)\quad \rho_0\left(\frac{\partial}{\partial t}+\boldsymbol{V}\cdot\nabla\right)\boldsymbol{v} \;=\; -\nabla p'\end{aligned} \tag{15}$$

By establishing a linear dependence between pressure and density for the sound wave:

$$p' \;=\; c^2\rho' \tag{16}$$

This enables us to rewrite equations (15) in the following way:

$$\begin{aligned}&(i)\quad \frac{1}{c^2}\left(\frac{\partial}{\partial t}+\boldsymbol{V}\cdot\nabla\right)p'+\rho_0\nabla\cdot\boldsymbol{v} \;=\; 0\\ &(ii)\quad \rho_0\left(\frac{\partial}{\partial t}+\boldsymbol{V}\cdot\nabla\right)\boldsymbol{v}+\nabla p' \;=\; 0\end{aligned} \tag{17}$$

Equation (17) (i) can be rearranged, whilst we can take the divergence from equation (17) (ii):

$$\begin{aligned}&(i)\quad \nabla\cdot\boldsymbol{v} \;=\; -\frac{1}{\rho_0 c^2}\left(\frac{\partial}{\partial t}+\boldsymbol{V}\cdot\nabla\right)p'\\ &(ii)\quad \rho_0\nabla\cdot\left[\left(\frac{\partial}{\partial t}+\boldsymbol{V}\cdot\nabla\right)\boldsymbol{v}\right]+\nabla^2 p' \;=\; 0\end{aligned} \tag{18}$$

Now the task is to prove that:

$$\nabla\cdot\left[\left(\frac{\partial}{\partial t}+\boldsymbol{V}\cdot\nabla\right)\boldsymbol{v}\right] \;=\; \left(\frac{\partial}{\partial t}+\boldsymbol{V}\cdot\nabla\right)(\nabla\cdot\boldsymbol{v}) \tag{19}$$

We cannot take the equality shown in (19) for granted; we need to prove it to use it. Let us start with the time derivative term, which is much easier than the one with the inner product. It is immediate that:

$$\nabla \cdot \left(\frac{\partial \boldsymbol{v}}{\partial t} \right) = \frac{\partial}{\partial t} (\nabla \cdot \boldsymbol{v}) \tag{20}$$

Because the partial time derivative is a linear operator (although I am not sure this is strictly needed) and mainly because the divergence is a derivative on position, and it will not interfere with the partial time derivative. So it is possible to reverse the order of the operations without changing the result. For the other term, we will need to do the operations explicitly and verify the equality.

3.3.1 Left-hand side of the equality of equation (19)

Let us start with:

$$\nabla \cdot \left[(\boldsymbol{V} \cdot \nabla) \boldsymbol{v} \right] \tag{21}$$

The first step is to apply the gradient operator on the vector $\boldsymbol{v}$. Before doing this, we need to understand some aspects of vector algebra. We write the vector in matrix form, given by:

$$\boldsymbol{v} = \begin{bmatrix} v_x \\ v_y \\ v_z \end{bmatrix} \tag{22}$$

When we write a vector in matrix form, we are already defining an coordinate orthonormal base to which the components depend on [21]. Here we decided to express the vector in Cartesian coordinates. Now we need to take the gradient of this vector. When we take the gradient of a scalar, what is obtained is a vector. By extending this reasoning, the gradient of a vector generates a second-rank tensor. This second-rank tensor can be obtained with the tensor product between two vectors, the gradient vector and the velocity vector[4] [22], [23]:

[4] The resulting tensor matrix is the transpose of the velocity gradient shown in [22]. But this is not a issue because both tensors are correct; their difference is just a matter of convention. Here we are being consistent with our definitions of vector and inner and outer products. And as it will be seen at the end, we will succeed in demonstrating the equality. Therefore our choices and definitions will also be correct.

$$\nabla \boldsymbol{v} = \underline{\underline{\nabla v}} \equiv \nabla \otimes \boldsymbol{v} = \nabla \boldsymbol{v}^T$$

$$\nabla \boldsymbol{v}^T = \begin{bmatrix} \frac{\partial}{\partial x} \\ \frac{\partial}{\partial y} \\ \frac{\partial}{\partial z} \end{bmatrix} \begin{bmatrix} v_x & v_y & v_z \end{bmatrix} = \begin{bmatrix} \frac{\partial v_x}{\partial x} & \frac{\partial v_y}{\partial x} & \frac{\partial v_z}{\partial x} \\ \frac{\partial v_x}{\partial y} & \frac{\partial v_y}{\partial y} & \frac{\partial v_z}{\partial y} \\ \frac{\partial v_x}{\partial z} & \frac{\partial v_y}{\partial z} & \frac{\partial v_z}{\partial z} \end{bmatrix} \tag{23}$$

The next step is to execute the inner product between the vector $\boldsymbol{V}$ and the second-rank tensor $\underline{\underline{\nabla v}}$. The inner product reduces the rank of the tensorial object, therefore, the result of this product is a vector [21]:

$$\boldsymbol{V} \cdot \underline{\underline{\nabla v}} = \boldsymbol{V}^T \underline{\underline{\nabla v}} = \begin{bmatrix} V_x & V_y & V_z \end{bmatrix} \begin{bmatrix} \frac{\partial v_x}{\partial x} & \frac{\partial v_y}{\partial x} & \frac{\partial v_z}{\partial x} \\ \frac{\partial v_x}{\partial y} & \frac{\partial v_y}{\partial y} & \frac{\partial v_z}{\partial y} \\ \frac{\partial v_x}{\partial z} & \frac{\partial v_y}{\partial z} & \frac{\partial v_z}{\partial z} \end{bmatrix}$$

$$\boldsymbol{V} \cdot \underline{\underline{\nabla v}} = \begin{bmatrix} V_x \frac{\partial v_x}{\partial x} + V_y \frac{\partial v_x}{\partial y} + V_z \frac{\partial v_x}{\partial z} \\ V_x \frac{\partial v_y}{\partial x} + V_y \frac{\partial v_y}{\partial y} + V_z \frac{\partial v_y}{\partial z} \\ V_x \frac{\partial v_z}{\partial x} + V_y \frac{\partial v_z}{\partial y} + V_z \frac{\partial v_z}{\partial z} \end{bmatrix} \tag{24}$$

At last, we need to take the divergence of such vector, finally getting a scalar:

$$\nabla\cdot\left(\boldsymbol{V}\cdot\underline{\underline{\nabla v}}\right) = \nabla^{T}\left(\boldsymbol{V}\cdot\underline{\underline{\nabla v}}\right)$$

$$\nabla\cdot\left(\boldsymbol{V}\cdot\underline{\underline{\nabla v}}\right) = \left[\frac{\partial}{\partial x}\quad\frac{\partial}{\partial y}\quad\frac{\partial}{\partial z}\right]\begin{bmatrix} V_x\frac{\partial v_x}{\partial x}+V_y\frac{\partial v_x}{\partial y}+V_z\frac{\partial v_x}{\partial z} \\ V_x\frac{\partial v_y}{\partial x}+V_y\frac{\partial v_y}{\partial y}+V_z\frac{\partial v_y}{\partial z} \\ V_x\frac{\partial v_z}{\partial x}+V_y\frac{\partial v_z}{\partial y}+V_z\frac{\partial v_z}{\partial z} \end{bmatrix} \tag{25}$$

$$\nabla\cdot\left(\boldsymbol{V}\cdot\underline{\underline{\nabla v}}\right) = V_x\frac{\partial^2 v_x}{\partial x^2}+V_y\frac{\partial^2 v_x}{\partial x\partial y}+V_z\frac{\partial^2 v_x}{\partial x\partial z}+V_x\frac{\partial^2 v_y}{\partial y\partial x}$$

$$+V_y\frac{\partial^2 v_y}{\partial y^2}+V_z\frac{\partial^2 v_y}{\partial y\partial z}+V_x\frac{\partial^2 v_z}{\partial z\partial x}+V_y\frac{\partial^2 v_z}{\partial z\partial y}+V_z\frac{\partial^2 v_z}{\partial z^2}$$

Therefore, the final expression can be written as:

$$\nabla\cdot\left(\boldsymbol{V}\cdot\underline{\underline{\nabla v}}\right) = \sum_{i,j=1}^{3} V_i\frac{\partial^2 v_j}{\partial x_j\partial x_i} \tag{26}$$

3.3.2 Right-hand side of the equality of equation (19)

We begin with:

$$\boldsymbol{V}\cdot\left[\nabla\left(\nabla\cdot\boldsymbol{v}\right)\right] \tag{27}$$

Applying the divergence operator on the vector $\boldsymbol{v}$ is very straight-forward:

$$\nabla\cdot\boldsymbol{v} = \left[\frac{\partial}{\partial x}\quad\frac{\partial}{\partial y}\quad\frac{\partial}{\partial z}\right]\begin{bmatrix} v_x \\ v_y \\ v_z \end{bmatrix} = \frac{\partial v_x}{\partial x}+\frac{\partial v_y}{\partial y}+\frac{\partial v_z}{\partial z} \tag{28}$$

Then we take the gradient of this scalar:

$$\nabla(\nabla\cdot\boldsymbol{v}) = \begin{bmatrix} \frac{\partial}{\partial x} \\ \frac{\partial}{\partial y} \\ \frac{\partial}{\partial z} \end{bmatrix} \left[\frac{\partial v_x}{\partial x} + \frac{\partial v_y}{\partial y} + \frac{\partial v_z}{\partial z} \right]$$

$$\nabla(\nabla\cdot\boldsymbol{v}) = \begin{bmatrix} \frac{\partial^2 v_x}{\partial x^2} + \frac{\partial^2 v_y}{\partial x \partial y} + \frac{\partial^2 v_z}{\partial x \partial z} \\ \frac{\partial^2 v_x}{\partial y \partial x} + \frac{\partial^2 v_y}{\partial y^2} + \frac{\partial^2 v_z}{\partial y \partial z} \\ \frac{\partial^2 v_x}{\partial z \partial x} + \frac{\partial^2 v_y}{\partial z \partial y} + \frac{\partial^2 v_z}{\partial z^2} \end{bmatrix} \tag{29}$$

Finally we perform the inner product between $\boldsymbol{V}$ and $\nabla(\nabla\cdot\boldsymbol{v})$:

$$\boldsymbol{V}\cdot\nabla(\nabla\cdot\boldsymbol{v}) = \begin{bmatrix} V_x & V_y & V_z \end{bmatrix} \begin{bmatrix} \frac{\partial^2 v_x}{\partial x^2} + \frac{\partial^2 v_y}{\partial x \partial y} + \frac{\partial^2 v_z}{\partial x \partial z} \\ \frac{\partial^2 v_x}{\partial y \partial x} + \frac{\partial^2 v_y}{\partial y^2} + \frac{\partial^2 v_z}{\partial y \partial z} \\ \frac{\partial^2 v_x}{\partial z \partial x} + \frac{\partial^2 v_y}{\partial z \partial y} + \frac{\partial^2 v_z}{\partial z^2} \end{bmatrix} \tag{30}$$

$$\boldsymbol{V}\cdot\nabla(\nabla\cdot\boldsymbol{v}) = V_x\frac{\partial^2 v_x}{\partial x^2} + V_x\frac{\partial^2 v_y}{\partial x \partial y} + V_x\frac{\partial^2 v_z}{\partial x \partial z} + V_y\frac{\partial^2 v_x}{\partial y \partial x} + V_y\frac{\partial^2 v_y}{\partial y^2}$$

$$+ V_y\frac{\partial^2 v_y}{\partial z \partial y} + V_z\frac{\partial^2 v_x}{\partial z \partial x} + V_z\frac{\partial^2 v_y}{\partial z \partial y} + V_z\frac{\partial^2 v_z}{\partial z^2}$$

This leads us to:

$$\boldsymbol{V}\cdot\nabla(\nabla\cdot\boldsymbol{v}) = \sum_{i,j=1}^{3} V_i \frac{\partial^2 v_j}{\partial x_i \partial x_j} \tag{31}$$

The order of the partial derivatives does not alter the final result, so we know that:

$$\sum_{i,j=1}^{3} V_i \frac{\partial^2 v_j}{\partial x_j \partial x_i} = \sum_{i,j=1}^{3} V_i \frac{\partial^2 v_j}{\partial x_i \partial x_j} \tag{32}$$

Finally, we can conclude that:

$$\nabla\cdot\left[(\boldsymbol{V}\cdot\nabla)\boldsymbol{v}\right] = \boldsymbol{V}\cdot\left[\nabla(\nabla\cdot\boldsymbol{v})\right] \tag{33}$$

Equation (19) is proven.

3.3.3 Final derivation of the wave equation

This means that we can write equation (18) (ii) in function of the divergence of $\boldsymbol{v}$:

$$\begin{aligned} &(i) \qquad \nabla\cdot\boldsymbol{v} \;=\; -\frac{1}{\rho_0 c^2}\left(\frac{\partial}{\partial t}+\boldsymbol{V}\cdot\nabla\right)p' \\ &(ii)\;\; \rho_0\left(\frac{\partial}{\partial t}+\boldsymbol{V}\cdot\nabla\right)(\nabla\cdot\boldsymbol{v}) + \nabla^2 p' \;=\; 0 \end{aligned} \tag{34}$$

Now we can substitute equation (34) (i) into (34) (ii):

$$-\frac{1}{c^2}\left(\frac{\partial}{\partial t}+\boldsymbol{V}\cdot\nabla\right)\left(\frac{\partial}{\partial t}+\boldsymbol{V}\cdot\nabla\right)p' + \nabla^2 p' \;=\; 0 \tag{35}$$

At this point, we need to look at the operator:

$$\left(\frac{\partial}{\partial t}+\boldsymbol{V}\cdot\nabla\right) \tag{36}$$

Is it linear? And the answer is yes. The partial time derivative is clearly a linear operator. The addition operation does not interfere with linearity. The $\boldsymbol{V}\cdot\nabla$ operator is also linear. The gradient is a linear operator, as it consist of first-order derivatives. The inner product with $\boldsymbol{V}$ is a linear operator as well. Thus, we conclude that the operator shown in expression (36) is linear, and we can apply it twice on a given scalar. This invites to write equation (35) as:

$$-\frac{1}{c^2}\left(\frac{\partial}{\partial t}+\boldsymbol{V}\cdot\nabla\right)^2 p' + \nabla^2 p' \;=\; 0 \tag{37}$$

Whence $\left(\frac{\partial}{\partial t}+\boldsymbol{V}\cdot\nabla\right)^2$ is the operator $\left(\frac{\partial}{\partial t}+\boldsymbol{V}\cdot\nabla\right)$ being applied on the scalar p' twice.

At last, we get the expression for the acoustic wave equation in a moving media, as in equation (11):

$$\frac{1}{c^2}\left(\frac{\partial}{\partial t}+\boldsymbol{V}\cdot\nabla\right)^2 p' \;=\; \nabla^2 p' \tag{38}$$

Note that even though this result was derived utilising Cartesian coordinates, it is also valid for cylindrical and spherical coordinates. This is important, because we will study the engine as an acoustic waveguide through cylindrical coordinates.

3.4 Derivation of the pressure function on the cylindrical waveguide

Starting from equation (38), we need first to define the direction of the velocity field of the moving fluid. We assume that it will have the form:

$$\boldsymbol{V} = c\,M\,\hat{\boldsymbol{k}} \tag{39}$$

With $\hat{\boldsymbol{k}}$ being the unit vector in the cylindrical z-axis. In this problem, in specific, we consider upstream sound propagation. Because we define sound will propagate in the positive direction of z-axis, the fluid motion will have the opposite direction. This can be expressed with a negative sign of Mach number M [4]. By developing the left-hand side of equation (38), we obtain:

$$\frac{1}{c^2}\left(\frac{\partial}{\partial t}+\boldsymbol{V}\cdot\nabla\right)^2 p' = \frac{1}{c^2}\left(\frac{\partial}{\partial t}+\boldsymbol{V}\cdot\nabla\right)\left(\frac{\partial}{\partial t}+\boldsymbol{V}\cdot\nabla\right)p' \tag{40}$$

At this point, it is important to be reminded that we are studying the problem with cylindrical coordinates. Thus, the gradient operator will also be presented with this choice of coordinates:

$$\boldsymbol{V}\cdot\nabla p' = \boldsymbol{V}^T\nabla p' = \begin{bmatrix}0 & 0 & cM\end{bmatrix}\begin{bmatrix}\frac{\partial p'}{\partial r}\\ \frac{1}{r}\frac{\partial p'}{\partial \theta}\\ \frac{\partial p'}{\partial z}\end{bmatrix} = cM\frac{\partial p'}{\partial z} \tag{41}$$

We find that:

$$\begin{aligned}&\frac{1}{c^2}\left(\frac{\partial}{\partial t}+\boldsymbol{V}\cdot\nabla\right)\left(\frac{\partial}{\partial t}+\boldsymbol{V}\cdot\nabla\right)p' = \frac{1}{c^2}\left(\frac{\partial}{\partial t}+\boldsymbol{V}\cdot\nabla\right)\left(\frac{\partial p'}{\partial t}+cM\frac{\partial p'}{\partial z}\right)\\ &=\frac{1}{c^2}\left(\frac{\partial}{\partial t}+cM\frac{\partial}{\partial z}\right)\left(\frac{\partial p'}{\partial t}+cM\frac{\partial p'}{\partial z}\right)=\frac{1}{c^2}\left[\frac{\partial^2 p'}{\partial t^2}+2cM\frac{\partial}{\partial t}\frac{\partial p'}{\partial z}+c^2M^2\frac{\partial^2 p'}{\partial z^2}\right]\end{aligned} \tag{42}$$

As for the right-hand side of equation (38), it is simply the Laplacian of the pressure in cylindrical coordinates:

$$\nabla^2 p' = \frac{1}{r}\frac{\partial}{\partial r}\left(r\frac{\partial p'}{\partial r}\right)+\frac{1}{r^2}\frac{\partial^2 p'}{\partial \theta^2}+\frac{\partial^2 p'}{\partial z^2} \tag{43}$$

And we can write equation (38) as:

$$\frac{1}{c^2}\left[\frac{\partial^2 p'}{\partial t^2}+2cM\frac{\partial}{\partial t}\frac{\partial p'}{\partial z}+c^2M^2\frac{\partial^2 p'}{\partial z^2}\right] = \frac{1}{r}\frac{\partial}{\partial r}\left(r\frac{\partial p'}{\partial r}\right)+\frac{1}{r^2}\frac{\partial^2 p'}{\partial \theta^2}+\frac{\partial^2 p'}{\partial z^2} \tag{44}$$

Assuming an harmonic motion, we have[5]:

$$\begin{aligned} p'(\boldsymbol{\eta},t) &= A e^{i(\omega t-\mathbf{k}\cdot\boldsymbol{\eta})} \\ \frac{\partial p'}{\partial t}(\boldsymbol{\eta},t) &= i\omega A e^{i(\omega t-\mathbf{k}\cdot\boldsymbol{\eta})} \\ \frac{\partial^2 p'}{\partial t^2}(\boldsymbol{\eta},t) &= -\omega^2 A e^{i(\omega t-\mathbf{k}\cdot\boldsymbol{\eta})} \end{aligned} \tag{45}$$

The resulting expressions are function of the wave frequency ω . As we saw in equation (7), the wave number depends on the frequency but also on geometrical variables, which in in this case we are yet to deduce. But [4] suggests us to substitute ω , perhaps to not have the differential equation in terms of time variables. And so we do, making the following substitution:

$$\omega = c k_0 \tag{46}$$

k_0 would be the wave number of the acoustic waves if there were not the geometrical constraints created by the waveguide, that is, if the wave could propagate in free space. The harmonic motion assumption enables us to free the differential equation from the time dependence, and we finally get the differential equation in function of the geometrical variables only:

$$-k_0^2 p' + 2ik_0 M\frac{\partial p'}{\partial z} + M^2\frac{\partial^2 p'}{\partial z^2} = \frac{\partial^2 p'}{\partial r^2} + \frac{1}{r}\frac{\partial p'}{\partial r} + \frac{1}{r^2}\frac{\partial^2 p'}{\partial \theta^2} + \frac{\partial^2 p'}{\partial z^2} \tag{47}$$

The solution for the differential equation can be expressed as a propagating wave in the z-axis, possessing the form:

$$p'(r,\theta,z,t) = \Phi(r,\theta)e^{-ik_z z}e^{i\omega t} \tag{48}$$

By applying this function into the differential equation, we obtain:

$$\frac{\partial^2\Phi}{\partial r^2} + \frac{1}{r}\frac{\partial\Phi}{\partial r} + \frac{1}{r^2}\frac{\partial^2\Phi}{\partial\theta^2} + \left(k_0^2 - k_z^2(1-M^2) - 2k_0 k_z M\right)\Phi = 0 \tag{49}$$

As in equations (4), we can solve equation (49) with separation of variables (the most formal solution would be to start with separation of variables from the beginning, equation (48), but as [4] does this way, we are reproducing these steps) . The method used here is very similar to that of quantum mechanics, when it is needed to solve the

[5] In physics books such as [16] and [18], the travelling wave is shown as $e^{i(\mathbf{k}\cdot\boldsymbol{\eta}-\omega t)}$, whilst in books such as [19], the latter an engineering book, the travelling wave is shown as $e^{i(\omega t-\mathbf{k}\cdot\boldsymbol{\eta})}$. Both expressions are equivalent, the difference of which is a π radians phase shift.

equations for the hydrogen atom. See [24]. Therefore, the incognito function can be written as:

$$\Phi(r,\theta) = R(r)\Theta(\theta) \tag{50}$$

The resulting differential equation, after some rearrangements, becomes:

$$\frac{r^2}{R}\left(\frac{d^2R}{dr^2}+\frac{1}{r}\frac{dR}{dr}\right)+\frac{1}{\Theta}\frac{d^2\Theta}{d\theta^2}+r^2k_{mn}^2 = 0 \quad , \qquad k_{mn}^2 = k_0^2-k_z^2\left(1-M^2\right)-2k_0k_zM \tag{51}$$

k_{mn} , with the indexes m and n ? We'll see why in a while. The term in the sum which depends on θ must be a constant, in order to hold the equality. This means that it can be written as:

$$\frac{1}{\Theta}\frac{d^2\Theta}{d\theta^2} = -m^2 \tag{52}$$

This leads to:

$$\Theta(\theta) = e^{im\theta} \quad \Leftrightarrow \quad \Theta(\theta) = A\cos(m\theta)+B\sin(m\theta) \quad , \quad m \in \mathbb{Z} \tag{53}$$

Because the function $\Theta(\theta)$ is periodic with period 2π . Now we are left with the differential equation for r :

$$\frac{r^2}{R}\left(\frac{d^2R}{dr^2}+\frac{1}{r}\frac{dR}{dr}\right)-m^2+r^2k_{mn}^2 = 0 \tag{54}$$

3.4.1 Bessel functions[6]

The following differential equation:

$$\frac{d^2y}{dx^2}+\frac{1}{x}\frac{dy}{dx}+\left(1-\frac{1}{x^2}\right)y = 0 \tag{55}$$

Appears in several branches of physics, and is very common when a problem is attacked through the method of separation of variables. In order to solve this equation, various approaches are possible. One of them is to propose a solution in the format of an infinite series:

[6] I owe professor Reginaldo de Jesus Napolitano from IFSC-USP my complete gratitude for providing me valuable observations on the study of Bessel functions which proved indispensable to writing this section.

$$y = \sum_{n=0}^{\infty} a_n x^n \tag{56}$$

By applying this solution into the equation, and equating coefficients of powers of x to zero, we get the following function [25]:

$$y = a_1\left(x - \frac{x^3}{2\cdot 4} + \frac{x^5}{2\cdot 4\cdot 4\cdot 6} - \frac{x^7}{2\cdot 4\cdot 6\cdot 4\cdot 6\cdot 8}\cdots\right) \tag{57}$$

This is a series called Bessel function, more precisely the Bessel function of the first kind. For the general differential equation, also called Bessel equation:

$$\frac{d^2 y}{dx^2} + \frac{1}{x}\frac{dy}{dx} + \left(1 - \frac{m^2}{x^2}\right)y = 0 \tag{58}$$

The Bessel function of order m is defined as [26]:

$$J_m(x) = \sum_{s=0}^{\infty} \frac{(-1)^s}{s!(m+s)!}\left(\frac{x}{2}\right)^{m+2s} = \frac{x^n}{2^n n!} - \frac{x^{n+2}}{2^{n+2}(n+1)!} + \cdots \tag{59}$$

Other approaches to get to the Bessel function involve a generating function or contour integrals, but will not be shown here. Bessel equation is a second-order differential equation and as such, it should involve the sum of two independent functions. For non-integral order ν, there are two independent solutions, namely, $J_\nu(x)$ and $J_{-\nu}(x)$, with ν replacing m in equation (59). But for integer m, the relevant case for this problem, it is not possible to get two independent solutions through the series method or the generating function. But a second solution exists, and it is called Neumann function or Bessel function of the second kind. It has the form [26]:

$$N_m(x) = -(n-1)!(2/x)^n/\pi + \cdots + \frac{2}{\pi}\left(\frac{x}{2}\right)^n \frac{1}{n!}\ln\left(\frac{x}{2}\right) + \cdots \tag{60}$$

Which has the remarkable characteristic of diverging to minus infinity for $x = 0$. Therefore, a Neumann function does not permit a finite solution at the origin. Considering that we want a finite value for the pressure field at the origin $r = 0$ for this waveguide, we rule out the Neumann function as a part of the solution for our differential equation due to the boundary conditions. Thus, the solution for the radial function $R(r)$ will only be composed of a Bessel function of the first kind, $J_m(x)$. For a cylindrical system of coordinates, the Bessel equation can be written as:

$$r^2 \frac{d^2}{dr^2} J_m(kr) + r \frac{d}{dr} J_m(kr) + (k^2 r^2 - m^2) J_m(kr) = 0 \tag{61}$$

In our problem, the function $R(r)$ will have the form:

$$R(r) = C J_m(k_{mn} r) \tag{62}$$

Like in equation (51), we are back with the indexes m and n of k_{mn}. We are yet to explain the index n. The other boundary condition is that the radial particle velocity on the wall must be zero [4]. This implies that the radial component of the pressure on the wall is null, what leads to the derivative of the pressure in relation to the radial position to zero:

$$\left.\frac{\partial p}{\partial r}\right|_{r=a} = \left.\frac{\partial \Phi}{\partial r}\right|_{r=a} = \left.\frac{dR}{dr}\right|_{r=a} = 0 \tag{63}$$

Thus, we have:

$$\left.\frac{dJ_m}{dr}(k_{mn} r)\right|_{r=a} = 0 \tag{64}$$

The derivative of the Bessel function can be expressed as:

$$\left.\frac{d}{dr}\left[\sum_{s=0}^{\infty} \frac{(-1)^s}{s!(m+s)!}\left(\frac{k_{mn} r}{2}\right)^{m+2s}\right]\right|_{r=a}$$

$$= \left.\sum_{s=0}^{\infty} \frac{(-1)^s}{s!(m+s)!} \frac{(m+2s) k_{mn}}{2}\left(\frac{k_{mn} r}{2}\right)^{m+2s-1}\right|_{r=a} \tag{65}$$

$$= \sum_{s=0}^{\infty} \frac{(-1)^s}{s!(m+s)!} \frac{(m+2s) k_{mn}}{2}\left(\frac{k_{mn} a}{2}\right)^{m+2s-1} = 0$$

There is an expression equal to zero and we can find ways to simplify it. We have already seen that m is an integer (equation (53)). Each m corresponds to a Bessel eigenfunction of order m. For a certain Bessel function, m is integer and thus fixed. This makes the factors $\frac{k_{mn}}{2}\left(\frac{k_{mn}}{2}\right)^m$ and $\left(\frac{a}{2}\right)^{m-1}$, at the last of equations (65), to be constants and this way they can be removed from the equation, unless k_{mn} and a are zero. The equation becomes:

$$\sum_{s=0}^{\infty} \frac{(-1)^s}{s!(m+s)!}(m+2s)\left(\frac{k_{mn}a}{2}\right)^{2s} = 0 \tag{66}$$

In order to solve the equation for this series, we can substitute the upper limit of the sum, infinity, for a positive integer number called N, as big as one wants. In such a case, we get the following equation for the variable k_{mn}:

$$\sum_{s=0}^{N} \frac{(-1)^s}{s!(m+s)!}(m+2s)\left(\frac{k_{mn}a}{2}\right)^{2s} = 0 \tag{67}$$

This means we have an equation of the degree $2N$, which leads to $2N$ roots for k_{mn}. In order to label each of the roots, we define firstly the constant m, because each order of the Bessel function will lead to different equations. For each value of m, as we saw, there are $2N$ roots. And each root will be given an index, called n, from the first (k_{m1}) to the 2N-th root of the equation (k_{m2N}). That is the reason the constant k, relative to the wave number of the acoustic waves in the waveguide, is given the index k_{mn} [7]. It is of fundamental importance to note that the index n refers to the number of the root of k_{mn}, from the smallest to the biggest, and it does not refer to the index s of the counting of the terms in the series. As we increase the size of N, more and more we get closer to the zeroes of the derivative of the Bessel function. For N at infinity, the solutions would converge to the zeroes of the derivative. These zeroes can be found through tables in the literature or by computational methods. Note! All zeros of the Bessel function and its derivatives, for $m \geqslant -1$ are real, but unfortunately we will not be able to prove that in this work. One point to be careful is that if one goes to a table to find the zeroes of the derivative of the Bessel function, he will find a quantity here labelled χ_{mn}, which relates with k_{mn} in the following way:

$$\chi_{mn} = k_{mn}\, a \tag{68}$$

This is because the argument of the Bessel function in the cylindrical choice of coordinates is $x = kr$, as seen in equation (61), and the tables are calculated for the argument of the Bessel function, and not for the argument divided by an arbitrary constant. In order to make this study more visual, let us show a graph of Bessel functions of the first kind for some orders:

[7] Actually, the most formal procedure would be not to label k as k_{mn} in equation (51) until we derived the reason why k has those indexes. But in order to be consistent with the notation of [4], we decided to put the indexes from the beginning.

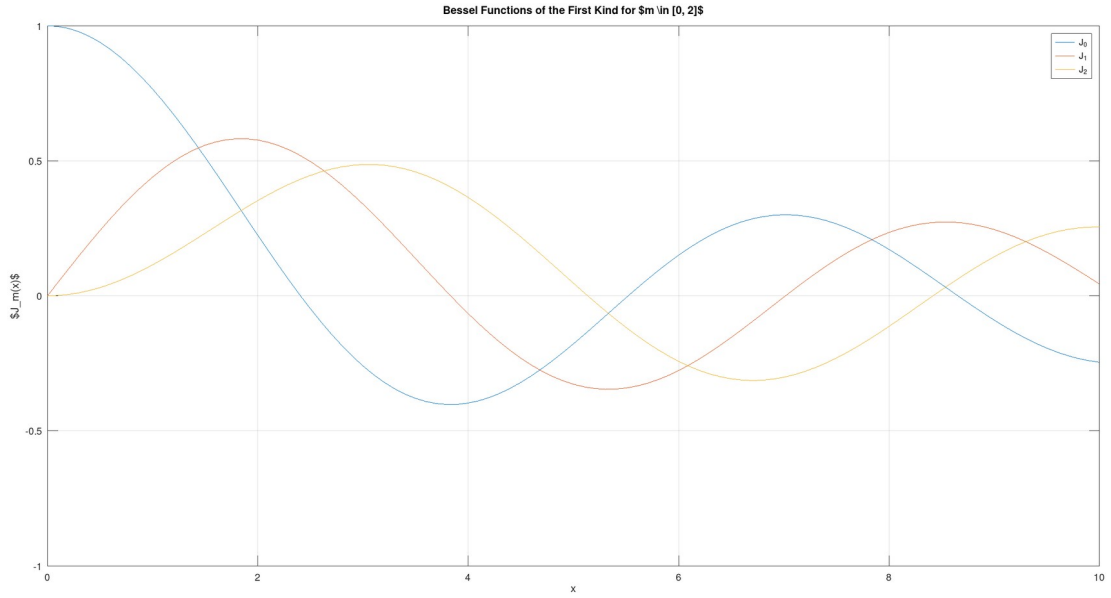

Fig. 23: Plots of Bessel functions of the first kind for the first integer orders
Source: see section 6 Appendices

By looking at this graph, we see that x_{01} , which is the same as χ_{01} , the first point at which the derivative of the Bessel function J_0 is zero, is at $x = 0.0$. If we refer to a table of zeroes of the Bessel function derivative, such as [27], we find that the position at which the derivative of the order zero Bessel function is null is at $x = 0.0$. But I must admit I cheated in this case. The picture is not clear as whether $x = 0$ is a point of zero derivative. The next point is clearer. We easily see that a point around $x = 3.9$ is a zero point for the derivative of J_0 , and as such, it would be labelled x_{02} , or χ_{02} . By looking at the table, we see that the actual point of zero derivative is at $x = 3.8317$. It was close, considering we estimated using our eyes. And so it goes on, if we cross-check the derivative zeroes of the graph against the tabulated values. In this way it is possible to have a more visual notion of what the points χ_{mn} mean. Note that we started our counting of n with $n = 1$. But this is just a matter of choice. In reference [4], the author starts with $n = 0$. Therefore, to be consistent with the notation of [4], we will take the first value of the integer n , which is related to the counting of the derivative zeroes in the Bessel function, as $n = 0$ onwards.

3.5 Wave propagation

We have successfully written all functions which compose the pressure field in relation to each coordinate variable thanks to the method of separation of variables. Now we shall write the expression for the function $\Phi(r,\theta)$:

$$\Phi(r,\theta) = \left[A_{mn}\cos(m\theta) + B_{mn}\sin(m\theta)\right]J_m(k_{mn}r) \tag{69}$$

Therefore, the pressure field is given by:

$$p'(r,\theta,z,t) = \left[A_{mn}\cos(m\theta) + B_{mn}\sin(m\theta)\right]J_m(k_{mn}r)e^{-ik_z z}e^{i\omega t} \tag{70}$$

The only incognito currently is k_z . But as we found the value of k_{mn} , k_z will be determined by solving the quadratic equation shown in equation (51):

$$k_{mn}^2 = k_0^2 - k_z^2(1-M^2) - 2k_0 k_z M \tag{71}$$

The solution of this equation is the following:

$$k_z = \frac{-Mk_0 \pm \sqrt{k_0^2 - k_{mn}^2(1-M^2)}}{(1-M^2)} \tag{72}$$

Thus, we see there are two solutions for the wave number in the z-axis, each corresponding to a travelling wave. In the same way as electromagnetic waves, which we studied in subsection 3.1, if the radicand in the square root assumes a negative value, there will be exponentially decaying pressure fields instead of a travelling wave. Likewise, we can define the cutoff frequency for wave propagation. The cutoff condition is given by:

$$k_0 = k_{mn}\sqrt{1-M^2} \tag{73}$$

Remember that we defined k_0 in equation (46) as ω / c . Therefore, the cutoff frequency is expressed as:

$$\omega_{cutoff} = c\,k_{mn}\sqrt{1-M^2} \tag{74}$$

An important remark on cutoff frequencies is that these pressure fields die because we are assuming an infinitely long cylindrical waveguide. In reality, that is not true and the nacelle has a finite length. This means that the waves with a frequency below the cutoff will dissipate exponentially but their modulus will not go to zero, as they travelled a finite length. When they leave the turbofan engine, these waves will propagate to the environment without attenuation, with a lower pressure than waves with frequencies above the cutoff. So the cutoff condition helps, but does not eliminate

lower-frequency wave propagation. How smaller the pressure field of those waves compared to non-cutoff waves would be is something that can be calculated considering the length of the turbofan and the path travelled by those waves.

Our initial equation in this problem was a Helmholtz equation (see equation (47)). The general solution for this equation is a linear combination of the product solutions, for the positive and negative values of k_z [28]:

$$\begin{aligned} p'(r,\theta,z,t) &= \sum_{m=0}^{N_\theta}\sum_{n=0}^{N_r}\left[A_{mn}^{(+)}\cos(m\theta)+B_{mn}^{(+)}\sin(m\theta)\right]J_m(k_{mn}r)e^{-ik_z^{(+)}z}e^{i\omega t} \\ &+ \sum_{m=0}^{N_\theta}\sum_{n=0}^{N_r}\left[A_{mn}^{(-)}\cos(m\theta)+B_{mn}^{(-)}\sin(m\theta)\right]J_m(k_{mn}r)e^{-ik_z^{(-)}z}e^{i\omega t} \end{aligned} \tag{75}$$

Any pressure field function can be written with this linear combination of functions, and the equation (75) is a double series, a Bessel-Fourier series. It is a Bessel series in r and a Fourier series in θ. If we know the pressure field for an harmonic acoustic wave, we can determine its coefficients for the Bessel-Fourier series in the following way:

$$\begin{aligned} \begin{Bmatrix} A_{mn} \\ B_{mn} \end{Bmatrix} &= 2\left[\pi a^2 e^{-ik_z z}e^{i\omega t}J_{m+1}^2(k_{mn})\right]^{-1} \\ &\cdot \int_0^{2\pi}\int_0^a p'(r,\theta,z,t)J_m(k_{mn}r)\begin{Bmatrix}\sin(m\theta)\\ \cos(m\theta)\end{Bmatrix} r\,dr\,d\theta \end{aligned} \tag{76}$$

Both Bessel and Fourier eigenfunctions are orthogonal [26]. Our final result, equation (75), is an important one. Remember that in section 2.1 we said that there are a lot of different sound-generating processes occurring inside the turbofan, which could be attributed to boundary layer phenomena and rotor-stator interaction, among others. In section 3.2 we said that if we are only interested in sound propagation, we did not need to be concerned with the source in the sound-generating processes. What we can make of this result is that if we make the assumption that the region V of the sound sources is small enough and we are only looking at sound propagation, then, no matter how complicated the sound-generating processes are at the sources, we can always represent the sound field inside the cylindrical waveguide (our model for the turbofan) as a double Bessel-Fourier series, because this representation encompasses all possible frequencies and amplitudes at the sound-generating processes inside the turbofan. The only issue is that we have a way to represent the sound field, but we do not know the

coefficients for the frequencies and amplitudes equation (75) in because we did not model the sound sources. But nonetheless equation (75) can be useful in our study of noise reduction by Herschel-Quincke waveguides.

4 Noise reduction on Herschel-Quincke waveguides

4.1 Theoretical modelling of the Herschel-Quincke waveguides

After we have defined the sound pressure field without the HQ waveguides, it is time to insert them in our theoretical model and see what conclusions of the behaviour of the system can be drawn. The first step is to define, in terms of a sound pressure field, what a Herschel-Quincke waveguide is.

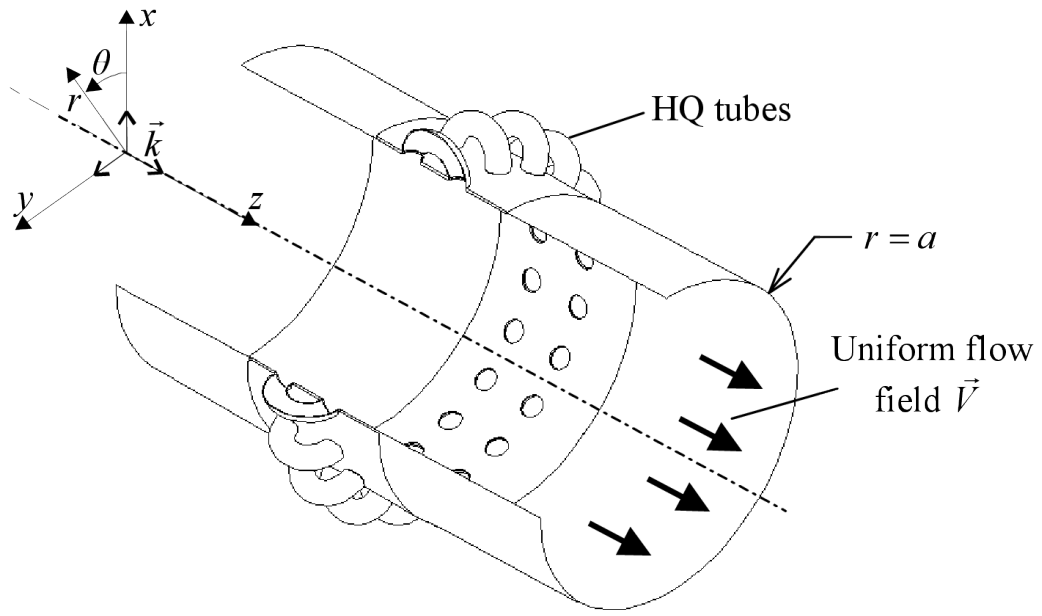

Fig. 24: HQ waveguides applied to the cylindrical waveguide
Source: [4]

According to [4] a reasonable model for a HQ waveguide would be a finite piston source. It is as if the cylindrical waveguide were permeated by several pistons in its wall, each with a definite position and producing a certain pressure field. The overall effect of a HQ waveguide could be simulated by adding the effects of all pistons around the circumference. The model for the HQ waveguides can be seen in Fig. 25. Now the need to define the pressure function for this finite piston source. The literature on the subject provides us several possible ways to express the pressure. According to Anselmet and Mattei [29], with a system of coordinates centred on the circular piston, its pressure in function of the position is given by:

$$p'(r,\theta) = \omega^2 \rho_0 u_0 R^2 \frac{e^{ikr}}{r} \frac{J_1\left[kR\sin(\theta)\right]}{kR\sin(\theta)} \tag{77}$$

It is important to note that the coordinates r and θ in equation (77) are not the same with which the analysis of the turbofan was made in subsection 3.4. The change of coordinates in this problem is not simple, because several assumptions were made in order to reach the form of the pressure field in (77). Because this is beyond the scope of this present work, the derivation of the pressure field for a certain position at the cylindrical wave guide will not be attempted at this work.

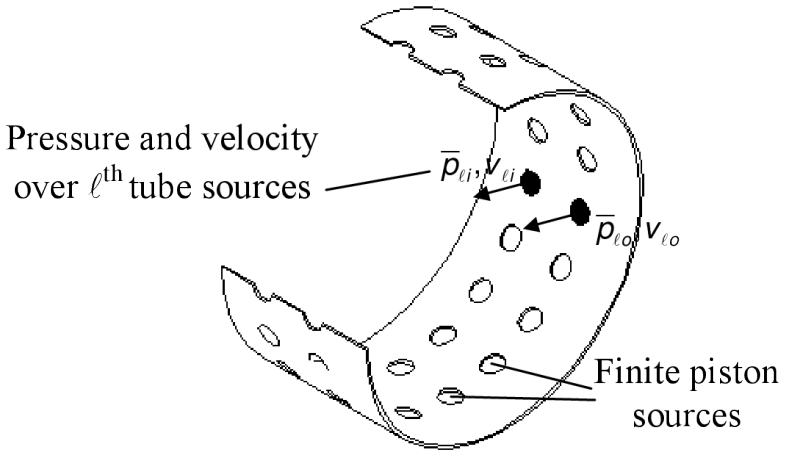

Fig. 25: Modelling HQ waveguides as finite piston sources
Source: [4]

Other author, Mangulis [30], for the similar problem of a circular rigid piston in a non-rigid baffle, presents us the following solution for the directivity and intensity of the pressure for such a system:

$$p'(r,\theta) = \frac{1}{2} R^2 u_0 \frac{e^{-ikr}}{r} \frac{\cos(\theta)}{\cos(\theta) - i\gamma} \frac{2J_1[kR\sin(\theta)]}{kR\sin(\theta)} \cdot \left\{ 1 - \gamma kR \sum_{m=0}^{\infty} c_m \frac{[kR\sin(\theta)]^2}{[kR\sin(\theta)]^2 - \lambda_m^2} \right\} \tag{78}$$

Now a solution presented by Morse and Ingard [31] for the problem of the radiation pressure generated by a circular piston:

$$p'(r,\theta) = -ik\rho c \frac{e^{ikr}}{4\pi r} 2u_\omega \pi R^2 \left\{ \frac{2J_1[kR\sin(\theta)]}{kR\sin(\theta)} \frac{\cos(\theta)}{\beta + \cos(\theta)} \right\} \tag{79}$$

Any of those pistons has a characteristic frequency, called ω or dependent on the wave number k. Therefore they can be considered, by themselves, sources of sound, because they are a resonant surface which has the capacity of modifying the pressure

field around. In the next section we are going to study in what ways those piston sources can attenuate noise from the cylindrical waveguide pressure field.

4.2 Noise attenuation by point sources of sound

In the last section, we argued that the Herschel-Quincke waveguides could be modelled as piston sources of sound and presented some possible formats for the pressure field they generate. Now we can assert that these sources of sound can also be considered points, what will be useful in our analysis because it makes the problem more tractable. The equation for the pressure field in the presence of a general source becomes [32]:

$$\frac{1}{c^2}\left(\frac{\partial}{\partial t}+\boldsymbol{V}\cdot\boldsymbol{\nabla}\right)^2 p' - \nabla^2 p' = f(r,\theta,z)e^{i\omega_0 t} \tag{80}$$

The fact that we have a term in the equation not dependent on p' makes it inhomogeneous, what invites us to the study of Green's functions.

4.2.1 Green's functions

Consider that we have a derivative operator called $\mathscr{L}$, which acts on a certain function $y(x)$. For a homogeneous differential equation, we would have the following:

$$\mathscr{L}\,y(x) = 0 \tag{81}$$

While a non-homogeneous differential equation would appear in this scenario:

$$\mathscr{L}\,y(x) = f(x) \tag{82}$$

Considering $f(x)$ a specified function of x. In the case of the inhomogeneous differential equation, equation (82) is equivalent to:

$$\mathscr{L}\,G(x,x') = \delta(x-x') \tag{83}$$

With δ being the Dirac delta function. Thus the solution for the non-homogeneous differential equation can be written as:

$$\begin{aligned} y(x) &= \int G(x,x')f(x')dx' \\ y(\boldsymbol{r_1}) &= \int G(\boldsymbol{r_1},\boldsymbol{r_2})f(\boldsymbol{r_2})d\,\tau_2 \end{aligned} \tag{84}$$

The latter of equations (84) is valid for $\Re^3$, a situation in three dimensions and three variables accordingly. G is called Green's function. This is a powerful

technique to solve inhomogeneous differential equations in several branches of physics [28], [33].

In our problem in aeroacoustics, the differential equation operator is:

$$\mathscr{L} = \nabla^2 - \frac{1}{c^2}\left(\frac{\partial}{\partial t} + \boldsymbol{V}\cdot\boldsymbol{\nabla}\right)^2 \tag{85}$$

This is a Helmholtz equation, albeit with a fluid velocity term $\boldsymbol{V}$. We can say that this operator is Hermitian, because, for an Hermitian operator:

1. The eigenvalues of an Hermitian operator are real. *In our operator, the eigenvalue is the constant* k_{mn} *found in equation (68). In that section, we have already said that the values of* k_{mn} *would be real.* Check.

2. The eigenfunctions of an Hermitian operator are orthogonal. *Our eigenfunction is the function of the Bessel-Fourier series presented in equation (75). And we have said that the eigenfunctions are orthogonal.* Check.

3. The eigenfunctions of an Hermitian operator form a complete set. *We did not prove this, but we provided the reference in section 3.5. Because both Fourier and Bessel series can form any function, then their product will also form a complete set* [34]. Check.

For an Hermitian operator, the Green's function can be written as:

$$G(\boldsymbol{r}_1, \boldsymbol{r}_2) = \sum_{n=0}^{\infty} \frac{\phi_n(\boldsymbol{r}_1)\,\phi_n(\boldsymbol{r}_2)}{\lambda_n - \lambda} \tag{86}$$

For the corresponding homogeneous differential equation:

$$\mathscr{L}\psi + \lambda\psi = 0 \tag{87}$$

Aimed at solving the inhomogeneous differential equation:

$$\mathscr{L}\psi + \lambda\psi = -\rho \tag{88}$$

4.2.2 Mechanism of sound attenuation

We learned that to find a determined function applied by an operator, we need to integrate the Green's function multiplied by a specific function (which generates the non-homogeneity) applied in the variable of the position of the source, what is demonstrated by equations (84). Now we are able to do this for a piston source in order to find the pressure field in the cylindrical waveguide. First we need to expand the source function $f(r,\theta,z)$ through a Fourier integral [32]:

$$f_{mn}(z) = \int_{-\infty}^{\infty} F_{mn}(k) e^{-ikz}\, dk \tag{89}$$

Note that, for the previous step, Plancherel's theorem was utilised to convert an integral in relation to a space variable into an integral in relation to the wave number k [35]. The function $F_{mn}(k)$ appears because we are already writing the eigenfunctions of the operator at the position of the source, such as equation (86) prescribes, but instead of having this eigenfunction in function of the position of the source z, we used Plancherel's theorem to have it in function of the wave number. Integration of Green's function leads to the following expression:

$$p'(r,\theta,z) = \sum_{m=0}^{\infty}\sum_{n=0}^{\infty} p_{mn}(r,\theta) \int_{-\infty}^{\infty} F_{mn}(k) \frac{e^{\left[i(\omega_0 t - kz)\right]}}{B_{mn}(\omega_0,k)}\, dk \quad ,$$

$$B_{mn}(\omega,k) = -\left(\frac{\omega}{c}\right)^2 + k_0{}^2 + \left(\frac{\omega_{mn}}{c}\right)^2 \tag{90}$$

If $\omega_{mn} > \omega_0$, the integral becomes exponentially small at large distances from the source region. Physically, we can say that then all motion in the mode p_{mn} has its energy trapped around the source. p_{mn} are the modes of the cylindrical waveguide in function of the general positional coordinate, that is, they are the representation of the pressure field of the turbofan engine. When there is a source function like $f(r,\theta,z)$, this source is capable to trap acoustic energy around it for values of frequency $\omega_{mn} > \omega_0$ [32]. In this way, a Herschel-Quincke waveguide, here modelled as a piston source, is capable to act as a noise attenuator.

The calculation presented in equation (90) is valid for a single piston source. As we have several pistons permeating the cylindrical waveguide, this integration would have to be performed as many times as the number of pistons. Even though it is in a certain

way implicit, it is this sum of each piston that creates the geometrical dependence of the distance between the pistons in the pressure field function. Because each piston is a source with a definite position, each integral will yield a different result and this enables us to quantify the effect of the distribution of the HQ waveguides in the cylindrical waveguide. In the first glance, this model does not present a dependence on the length of the HQ waveguides; however, the velocity of the piston and its frequency, two variables in our piston model, possibly have a mathematical relation with the length of the HQ waveguide.

5 Conclusion

In this work, we presented the problem of sound noise generated at the inlet of the turbofan engine. In order to understand better the mechanisms of sound generation, the turbofan and its parts were introduced, followed by technologies currently utilised in order to reduce sound pollution generation, such as lobular mixers and chevron nozzles. We also emphasised liner technology and distinguished the absorber and resonant types of sound absorbers.

Then the Herschel-Quincke technique was introduced, and we drew a timeline showing the advancements in its study along the centuries. The experimental study of Burdisso and Smith [13] showing the potential of the Herschel-Quincke waveguides in reducing noise from the turbofan inlet was presented in fine detail, as well as the results obtained.

Afterwards, a theoretical study of the turbofan engine was carried based on the theory of waveguides. Firstly, as a source of inspiration, the theory of electromagnetic waveguides was derived and its properties and the mathematics involving them was investigated. The most remarkable points in that study were the concept of cutoff frequency and the mathematical technique of separation of variables to solve partial differential equations.

Finally the turbofan engine was modelled as a cylindrical waveguide. Because of the airflow, a velocity term had to be added to the acoustic equations for the pressure field. Starting from Navier-Stokes equations, we derived the acoustic equation for the pressure field in moving media with the use of theory of tensors and vector calculus. After this study, we were finally able to find the differential equation for the pressure field. It was solved in a similar way as in the electromagnetic case, but this time, because the waveguide was cylindrical, we also had to solve Bessel’s differential equation. In order to do so, the concept of Bessel functions had to be introduced, and enabled us to understand the mathematical meaning of the eigenvalues for the wave number. We then were able to present a final expression for the pressure field encompassing all kinds of sound-generating processes, by being a complete Bessel-Fourier series.

At last we attempted to understand theoretically in what ways Herschel-Quincke waveguides can have a noise attenuating effect on a turbofan. For this we had to model those waveguides as finite piston sound sources, and we presented, based on the work of different authors, several models for the sound field this piston would generate. Because the introduction of the piston source would create a inhomogeneity in the differential equation for the pressure field, we had to introduce the concept of Green's functions. Armed with this important technique for solving inhomogeneous differential equations, we were able to demonstrate how the point sound source would be able to trap certain pressure modes at the waveguide, thus being able to reduce noise propagation.

This work is far from being complete, and as future improvements, one could better develop the Green's functions for sound propagation in this waveguide, present the piston sources in the general coordinates of the system and even carry out calculations to make a theoretical prediction of noise reduction in decibels. Later, a computational numerical simulation could be performed in order to compare the theory with experiments. There are some aspects of the eigenfunctions and their orthogonality which were not completed explored in this work and one would be welcome to further advance on the subject.

6 Appendices

Appendix I: MATLAB/Octave code of the Bessel functions plot

```
x = 0:0.1:10;
J = zeros(3,101);

for i = 0:2
    J(i+1,:) = besselj(i,x);
end

plot(x,J)
grid on
legend('J_0','J_1','J_2','Location','Best')
title('Bessel Functions of the First Kind for $m \in [0, 2]$','interpreter','latex')
xlabel('x','interpreter','latex')
ylabel('$J_m(x)$','interpreter','latex')

```

7 Bibliography

[1] J. F. Marchman III. “Propulsion” in *Aerodynamics and Aircraft Performance*, 3rd ed. Blacksburg, VA, USA, James F. Marchman III in association with the University Libraries at Virginia Tech, 2021. [Online]. Available: https://pressbooks.lib.vt.edu/aerodynamics

[2] E. Kappos, “Robust multivariable control for the F100 engine”, M.S. thesis, Massachusetts Inst. of Tech., Cambridge, MA, USA, 1983, ch. 2, pp. 18. [Online]. Available: https://dspace.mit.edu/handle/1721.1/15487

[3] J. M. Tyler and T. G. Sofrin, “Axial Flow Compressor Noise Studies”, SAE Technical Paper 620532, 1962, doi: 10.4271/620532.

[4] R. F. Hallez, “Investigation of the Herschel-Quincke Tube Concept as a Noise Control Device for Turbofan Engines”, M.S. thesis, Virginia Poly. Inst. and State Univ., Blacksburg, VA, USA, 2001, ch. 2, pp. 11-38. [Online]. Available: https://vtechworks.lib.vt.edu/handle/10919/31081

[5] W. Yingjun, G. Minghao and H. Yu, “CJ-3000 Turbofan Engine Design Proposal”, AIAA Foundation Undergraduate Team Engine Design Competition, 2017-18, ch. 11, pp. 37-8. [Online]. Available: https://www.aiaa.org/get-involved/students-educators/Design-Competitions/2017-2018-design-competition-winning-reports#engine-design-competitions-%E2%80%93-candidate-engines-for-next-generati

[6] T. Barber, “Turbofan Forced Mixer Lobe Flow Modeling – II - Three-Dimensional Inviscid Mixer Analysis (FLOMIX)”, NASA Contractor Report 4147, 1988. [Online]. Available: https://ntrs.nasa.gov/api/citations/19890004851/downloads/19890004851.pdf

[7] Apparatus for linear actuation of flow altering components of jet engine nozzle, by D. P. Calder and P. Bhutiani. (2022, Aug., 24). European Patent EP2535547 [Online]. Available: https://data.epo.org/gpi/EP2535547A2

[8] R. Ji, X. Huang, and X. Zhao, “Active Jet Noise Control of Turbofan Engine Based on Explicit Model Predictive Control,” *Applied Sciences*, vol. 12, no. 10, p. 4874, May 2022, doi: 10.3390/app12104874.

[9] A. P. Dowling and J. E. Ffowcs Williams. “Sound Waves Incident on a Flat Surface of Discontinuity” in *Sound and Sources of Sound*. Ellis Horwood Limited, 1983, ch. 4, pp. 83-5.

[10] R. Xue, C. M. Mak, C. Cai, and K. W. Ma, “An Infinity Tube with an Expansion Chamber for Noise Control in the Ductwork System,” *Sensors*, vol. 23, no. 1, p. 305, Dec. 2022, doi: 10.3390/s23010305.

[11] Z. Zhichi, L. Song, T. Rui, G. Rui, D. Genhua and L. Peizi, “Application of Quincke tubes to flow ducts as a sound attenuation device”, *Noise Control Eng. J.*, vol. 46, no. 6, pp. 245-55, Nov-Dec 1998, doi: 10.3397/1.2828476.

[12] A. Selamet, N. S. Dickey, and J. M. Novak, “The Herschel–Quincke tube: A theoretical, computational, and experimental investigation", *J. Acoust. Soc. Am.*, vol. 96, no. 5, pp. 3177–3185, Nov. 1994. doi: 10.1121/1.411255.

[13] R. A. Burdisso and J. P. Smith, ‘Control of inlet noise from turbofan engines using Herschel-Quincke waveguides’, *6th Aeroacoustics Conference and Exhibit*. *American Institute of Aeronautics and Astronautics*, Jun. 12, 2000. doi: 10.2514/6.2000-1994.

[14] L. A. Brady, “Application of the Herschel-Quincke Tube Concept to Higher-Order Acoustic Modes in Two-Dimensional Ducts”, M.S. thesis, Virginia Poly. Inst. And State Univ., Blacksburg, VA, USA, 2002. [Online]. Available: https://vtechworks.lib.vt.edu/handle/10919/31479

[15] R. P. Feynman. “Waveguides” in *The Feynman Lectures on Physics*. [Online]. Available: https://www.feynmanlectures.caltech.edu/II_24.html. [Accessed 21 May 2023].

[16] D. J. Griffiths. “Electromagnetic waves” in *Introduction to Electrodynamics*, 3rd ed. Prentice Hall, 1999, ch. 9, pp. 405-10.

[17] A. P. Dowling and J. E. Ffowcs Williams. “Sources of Sound” in *Sound and Sources of Sound*. Ellis Horwood Limited, 1983, ch. 7, pp. 148.

[18] P. M. Morse and K. U. Ingard. “Acoustics in Moving Media” in *Theoretical Acoustics*. Princeton University Press, 1987, ch. 11, pp. 698-701.

[19] A. P. Dowling and J. E. Ffowcs Williams. “Three-Dimensional Sound Waves” in *Sound and Sources of Sound*. Ellis Horwood Limited, 1983, ch. 2, pp. 37.

[20] M. S. Howe. “Introduction” in *Theory of Vortex Sound*. Cambridge University Press, 2003, ch. 1, pp. 3.

[21] W. Herreman. (2021). Mécanique des fluides, pp. 122-3. [Online]. Available: https://perso.limsi.fr/wietze/cours/MF/meca_flu_poly2021-2022.pdf

[22] W. Herreman. (2021). Mécanique des fluides, pp. 11-2. [Online]. Available: https://perso.limsi.fr/wietze/cours/MF/meca_flu_poly2021-2022.pdf

[23] Ø. Ryan, G. Dahl, and K. Mørken. (2012). Fourier theory, wavelet analysis and nonlinear optimization, pp. 214. [Online]. Available: https://www.uio.no/studier/emner/matnat/math/nedlagte-emner/MAT-INF2360/v12/siglinbok.pdf

[24] D. J. Griffiths. “Quantum Mechanics in Three Dimensions” in *Introduction to Quantum Mechanics,* 2nd ed. Pearson Prentice Hall, 2005, ch. 4, pp. 131-60.

[25] P. M. Morse and K. U. Ingard. “Introductory” in *Theoretical Acoustics*. Princeton University Press, 1987, ch. 1, pp. 6-8.

[26] G. B. Arfken and H. J. Weber. “Bessel Functions” in *Mathematical Methods for Physicists*, 4th ed. Academic Press, Inc., 1995, ch. 11, pp. 627-56.

[27] P. M. Morse and K. U. Ingard. “Tables of Functions” in *Theoretical Acoustics*. Princeton University Press, 1987, Table X, Zeros of Bessel Functions, pp. 902.

[28] G. B. Arfken and H. J. Weber. “Differential Equations” in *Mathematical Methods for Physicists*, 4th ed. Academic Press, Inc., 1995, ch. 8, pp. 456-536.

[29] F. Anselmet and P.-O. Mattei, “Radiation, Diffraction, Enclosed Space” in *Acoustics, Aeroacoustics and Vibrations*, ISTE Ltd and John Wiley & Sons, Inc., 2016, ch. 5, pp. 105-64.

[30] V. Mangulis, ‘Radiation of sound from a circular rigid piston in a nonrigid baffle’, *Int. J. of Engng. Sci.*, vol. 2, no. 1. Elsevier BV, pp. 115–127, Apr. 1964. doi: 10.1016/0020-7225(64)90013-8.

[31] P. M. Morse and K. U. Ingard. “The Radiation of Sound” in *Theoretical Acoustics*. Princeton University Press, 1987, ch. 7, pp. 381.

[32] J. Lighthill, “Internal Waves” in *Waves in Fluids.* Cambridge University Press, 1978, ch. 4, pp. 418-31.

[33] A. P. Young. (2013). Solution of inhomogeneous differential equations using Green functions. [Online]. Available: https://young.physics.ucsc.edu/116C/gf.pdf

[34] G. B. Arfken and H. J. Weber. “Sturm-Liouville Theory - Orthogonal Functions” in *Mathematical Methods for Physicists*, 4th ed. Academic Press, Inc., 1995, ch. 9, pp. 537-90.

[35] D. J. Griffiths. “Time-Independent Schrödinger Equation” in *Introduction to Quantum Mechanics,* 2nd ed. Pearson Prentice Hall, 2005, ch. 2, pp. 24-92.